Published online 4 March 2020

Nucleic Acids Research, 2020, Vol. 48, No. 7 ***3657–3677***
doi: 10.1093/nar/gkaa138

SV40 T antigen interactions with ssDNA and replication protein A: a regulatory role of T antigen monomers in lagging strand DNA replication

Nichodemus O. Onwubiko[1,†], Angela Borst[2,†], Suraya A. Diaz[1,†], Katharina Passkowski[2,†], Felicia Scheffel[2,†], Ingrid Tessmer[2,*] and Heinz P. Nasheuer[1,*]

[1]Biochemistry, School of Natural Sciences, Center for Chromosome Biology, Biomedical Sciences Building, NUI Galway, New Castle Road, Galway, Ireland and [2]Rudolf Virchow Center for Experimental Biomedicine, University of Würzburg, Josef Schneider Strasse 2, 97080 Würzburg, Germany

Received January 10, 2020; Revised February 14, 2020; Editorial Decision February 17, 2020; Accepted February 26, 2020

ABSTRACT

DNA replication is a central process in all living organisms. Polyomavirus DNA replication serves as a model system for eukaryotic DNA replication and has considerably contributed to our understanding of basic replication mechanisms. However, the details of the involved processes are still unclear, in particular regarding lagging strand synthesis. To delineate the complex mechanism of coordination of various cellular proteins binding simultaneously or consecutively to DNA to initiate replication, we investigated single-stranded DNA (ssDNA) interactions by the SV40 large T antigen (Tag). Using single molecule imaging by atomic force microscopy (AFM) combined with biochemical and spectroscopic analyses we reveal independent activity of monomeric and oligomeric Tag in high affinity binding to ssDNA. Depending on ssDNA length, we obtain dissociation constants for Tag-ssDNA interactions (K_D values of 10–30 nM) that are in the same order of magnitude as ssDNA binding by human replication protein A (RPA). Furthermore, we observe the formation of RPA-Tag-ssDNA complexes containing hexameric as well as monomeric Tag forms. Importantly, our data clearly show stimulation of primase function in lagging strand Okazaki fragment synthesis by monomeric Tag whereas hexameric Tag inhibits the reaction, redefining DNA replication initiation on the lagging strand.

INTRODUCTION

The replication of cellular DNA is a central process and similar mechanisms have evolved for DNA replication in all living organisms (1–4). Studies to understand eukaryotic DNA replication are at the forefront of molecular biological research. Our knowledge of eukaryotic DNA replication has made progress at all levels thanks to the use of biochemical and biological model systems (2,4,5). Due to their largely comparable but simplified replication machinery, the small double-stranded DNA viruses of the polyomavirus family represent a highly suitable model for the more complex eukaryotic system. These viruses have yielded numerous important insights into the mechanisms of eukaryotic DNA replication (6–9). Nevertheless, the mechanism of eukaryotic DNA replication is still only partially understood (2,4).

Simian virus 40 (SV40) is a particularly prominent, well-studied member of the polyomavirus family. The SV40 genome is organized in three specific areas: (i) a non-coding control region (NCCR) which includes the origin of DNA replication, (ii) the early genes which code for large T antigen (Tag) and small t antigen, and (iii) the late genes encoding the capsid proteins VP-1, VP-2 and VP-3, and the agnoprotein (6,10,11). SV40 DNA replication requires the viral replication origin, which is localized in the NCCR, and only one viral protein, the multifunctional Tag helicase, with the host supplying all other replication factors. *In vivo*, DNA replication depends in addition on SV40 small t antigen but the exact role of this protein factor is not fully understood (6,7,9,10,12,13). The model of replication in SV40 is consistent with eukaryotic cellular chromosomal DNA replication in S phase with two exceptions. Firstly, the activities of SV40 Tag do not require the multitude of protein

*To whom correspondence should be addressed. Tel: +353 91 492430; Fax: +353 91 495504; Email: h.nasheuer@nuigalway.ie
Correspondence may also be addressed to Ingrid Tessmer. Tel: +49 931 31 80425; Fax: +49 931 31 87320; Email: Ingrid.tessmer@virchow.uni-wuerzburg.de
†The authors wish it to be known that, in their opinion, the first five authors should be regarded as Joint First Authors.

factors necessary in eukaryotic cellular DNA replication, such as the origin recognition complex (ORC), the helicase-loading factors Cdc6 and Cdt1, and the replicative helicase that consists of the CMG complex composed of Cdc45, the Mcm2-7 helicase core complex and the GINS complex (2,14–16). Secondly, DNA polymerase δ (Pol δ) carries out leading and lagging strand DNA synthesis in the SV40 system whereas in cellular DNA replication these functions are shared between Pol ε on the leading and Pol δ on the lagging strand DNA (2,14,15). SV40 DNA replication is hence a good model to understand the intricate and complex eukaryotic system.

During initiation of DNA replication, SV40 Tag binds to the core origin, which contains the early palindrome, an AT-rich sequence, and the Tag-binding site 2. The latter consists of two pairs of G(G/A)GGC penta-nucleotides (10). In the presence of ATP Tag forms a double-hexamer on the core origin and partially melts, the early palindrome (EP) as well as untwists the AT-rich sequence of the SV40 origin (7,17–19). In the next steps Tag double-hexamers bidirectionally unwind the viral replication origin in an ATP hydrolysis-dependent manner (8,20,21). During the further unwinding of the double-stranded DNA (dsDNA), the two Tag hexamers may dissociate from each other due to phosphorylation of S120 and S123 and move along the leading strand in 3′ to 5′ direction with the separated two single-stranded DNAs (ssDNAs) threaded through their hexameric channels (7,8). SV40 Tag unwinding of the core origin and its flanking sequences results in long stretches of ssDNA and in downstream torsional stress in the DNA that necessitate two further protein factors. The emerging ssDNA is protected by replication protein A (RPA), the main eukaryotic ssDNA-binding protein, which binds the DNA with the help of Tag (6,22–25). Topoisomerase I releases the resulting torsional stress, enhancing initiation of DNA replication (17,26). To start DNA synthesis, DNA polymerase α-primase (Pol-prim) is loaded onto this Tag-RPA-topoisomerase I DNA complex establishing a functional SV40 replication initiation complex (7–9,26,27). In a species-specific manner, human Pol-prim synthesizes short RNA primers in the SV40 origin, which are elongated by the DNA polymerase function of the enzyme complex (2,8,15,28,29). After a polymerase switch from Pol-prim to Pol δ, which is supported by RPA, replication factor C (RFC) and proliferating cell nuclear antigen (PCNA), Pol δ associated with PCNA synthesizes leading strand DNA in a processive fashion (9,15,30–34). In contrast, lagging strand synthesis is discontinuous and Pol-prim in complex with Tag catalyzes the multiple initiation events on the RPA-bound ssDNA (27,35–37). The DNA polymerase function of Pol-prim then elongates the RNA primers and produces RNA-DNA primers (38,39). Similar as for leading strand synthesis, Pol δ then synthesizes the complete Okazaki fragments after a polymerase switch (2,15,30–33). The maturation of these Okazaki fragments requires the collaboration of RNase H, PCNA, Fen 1, Pol δ and DNA ligase I to establish a continuous strand on the lagging strand (2,14,16,40,41).

The central role of Tag in SV40 DNA replication initiation is indisputable (6,10). It is required for origin recognition, DNA unwinding, RPA and DNA polymerase recruitment. While Tag binding to dsDNA with or without the core origin sequence has been excessively studied (8,11,17–21,42–47), Tag interactions with ssDNA have been explored relatively little, and mostly with the isolated N-terminal origin binding domain (OBD) (48–51) or C-terminal helicase domain (48–52). Similarly, the physical and functional interactions of RPA to stimulate the initiation of lagging strand synthesis of the Okazaki fragments by the primase function of Pol-prim in the origin of DNA replication is still not completely understood (6,24,35,36,39). Recently published reports showed that in cell-free systems Okazaki fragment synthesis is much less efficient than leading strand synthesis (53). Additional factors are therefore required or known factors used in these systems are present in less than optimal concentrations including factors associated with chromatin (54).

Here, we investigate in detail the properties of full-length Tag binding to ssDNA to delineate the complex mechanism of coordination of various cellular proteins binding simultaneously or consecutively to DNA to initiate replication (46,49–52,55). In particular, we focus on the coordinated interaction of Tag and RPA with ssDNA, which has been shown to enhance primase function (35–37,56,57). Using single molecule imaging by atomic force microscopy (AFM) combined with biochemical, sedimentation, and spectroscopic analyses we characterize the involved protein-protein and protein-DNA interactions. Importantly, our data reveal a function for monomeric Tag protein binding to ssDNA in stimulating of Pol-Prim activity during initiation of DNA synthesis on un-primed ssDNA bound by RPA, a model system for the initiation of Okazaki fragment synthesis, whereas hexameric/double-hexameric Tag complexes inhibit the process. From our data we developed a model of the role and interplay of Tag and RPA in SV40 DNA replication initiation. Our model may be applied to eukaryotic replication, replacing Tag by the complex protein systems of the eukaryotic replicative helicase CMG complex with diverse co-factors. We will discuss interesting analogies between Tag-RPA-primase interactions and initiation of primase function in virus and eukaryotes.

MATERIALS AND METHODS

Protein expression and purification

SV40 T antigen (Tag, $M_r \sim 81\,580$ Da) was expressed using a baculoviral expression system as described elsewhere (58,59). Briefly, High Five® insect cells (Invitrogen) at a concentration of 1×10^7 cells/ml were infected for 44 h with 10 PFU per cell of recombinant baculovirus expressing SV40 Tag. The cells were harvested and washed in cold PBS at $350\times g$ for 5 min at 4°C and homogenized with tight pestle in 30 mM HEPES–KOH, pH 7.8, 0.5% NP-40, 150 mM NaCl and 1× EDTA-free protease inhibitors (Sigma) (buffer A) (5 ml of lysis buffer A was added to 1 g of cells pellet). The lysate was clarified by centrifugation at $30\,000\times g$ for 30 min at 4°C and the supernatant was then applied to pre-equilibrated HIS-Select® Nickel Affinity Gel (Sigma) in 30 mM HEPES–KOH, pH 7.8, 150 mM NaCl and 1× EDTA free protease inhibitors (buffer B) for 1 h. Subsequently the resin was washed with 30 column volumes of buffer B and SV40 Tag was eluted in 30 mM HEPES–KOH, pH 7.8, 150 mM NaCl, 250 mM Imidazole and 1× EDTA

free protease inhibitors (buffer C). The eluted SV40 Tag was concentrated using Vivaspin concentrators with a 10 kDa molecular weight cut-off (Sartorius) and the buffer exchanged to buffer B using PD-10 desalting columns (GE Healthcare) according to the manufacturers' instructions. The extracted SV40 Tag was stored at −80°C and examined by SDS-PAGE (Hoefer) followed by Coomassie Brilliant blue staining or western blotting. SDS-PAGE analysis indicated that SV40 Tag was approximately 95% pure. Protein concentrations were determined by UV absorbance spectrophotometry using a NanoDrop 2000 Spectrophotometer (Thermo Fisher Scientific). Absorbance spectra were collected from 250 to 300 nm. Tag concentration was calculated from the reading at 280 nm using a molar extinction coefficient of $\varepsilon_{280\,nm} = 104{,}125\ M^{-1}\ cm^{-1}$, and confirmed by Bradford assay (Bio-Rad).

In addition, Tag was expressed and purified from *Escherichia coli* (*E. coli*) culture as a shortened construct ($Tag_{131–627}$), as previously described by Chang *et al.* (21). Shortly, $Tag_{131–627}$ was produced containing a wild type Tag sequence and as variants with mutations in the dimerization interface $Tag_{131–627}$ (V350E/P417D) and $Tag_{131–627}$ (L286D/R567E), which results in exclusively monomeric Tag proteins. The DNA sequences for wild type and monomer $Tag_{131–627}$ (V350E/P417D) were synthesized and cloned into the pGex-6P-1 by GenScript Biotech (Leiden, Netherlands) whereas monomer $Tag_{131–627}$ (L286D/R567E) was cloned into vector pETM41 to express the protein as 6xHis-maltose binding protein FLAG tag fusion protein. The fusion proteins were expressed using *E. coli* BL21-CodonPlus (DE3)-RIL cells (Agilent Technologies, UK). Bacteria were grown to a $OD_{600\,nm} = 0.2$ at 37°C in LB media with 350 mM NaCl, and then transfer to a shaker at 16°C. Induction of protein expression was carried out with 0.2 mM IPTG overnight for 18 h and the cells were harvested. The cells were lysed in lysis buffer (50 mM Tris–HCl, pH 8.0, 0.25 M NaCl, 10 mM DTT, 1 mM EDTA) using sonication. Affinity purification was carried out using buffer A (50 mM Tris–HCl, pH 8.0, 0.25 M NaCl, 1 mM DTT, 1 mM EDTA) and GST resin (GE Healthcare), wild type and monomer mutant $Tag_{131–627}$ (V350E/P417D), or nickel chelating chromatography, monomer mutant $Tag_{131–627}$ (L286D/R567E) using buffer B (50 mM Tris–HCl, pH 8.0, 0.25 M NaCl, 1 mM DTT). The fusion proteins were cleaved with precision protease or TEV protease and the partially purified proteins were further enriched by size exclusion chromatography (SEC) using a Superdex 200 16/600 PG (GE Healthcare). Tag-containing fractions were concentrated using Vivaspin concentrators and snap-frozen. $Tag_{131–627}$ concentrations were calculated from the reading at 280 nm using a molar extinction coefficient of $\varepsilon_{280nm} = 64\,290\ M^{-1}\ cm^{-1}$. The proteins were more than 95% pure and, consistent with a previous report (21), recombinant wild type $Tag_{131–627}$ formed monomers and hexamers in solution whereas recombinant mutant $Tag_{131–627}$ (V350E/P417D) and FLAG-$Tag_{131–627}$ (L286D/R567E) protein exclusively formed monomers as determined by SEC (data not shown).

Human RPA was expressed in *E. coli* as heterotrimeric complex and purified as previously described (36,60–62).

DNA substrates

In the differential scanning fluorimetry (DSF) and electromobility shift assay (EMSA) experiments, two different 57-mer DNA oligonucleotides with or without complementary DNA sequences were employed (Supplemental Table S1); ssDNA(GAPDH) (5′-CGA CAG TCA GCC GCA TCT TCT TTT GCG TCG CCA GCC GAG CCC TAT AGT GAG TCG TAT-3′) and an SV40 Tag recognition site 2 sequence-containing oligonucleotide, ssDNA(Site2), 5′-GCT CAG AGG CCG AGG CGG CCT CGG CCT CTG CAT AAA TAA AAA AAA TTA GTC AGC CAT-3′. The oligonucleotide ssDNA(Site2) sequence comprises the lower strand of the SV40 origin of replication from position 5227 to 40 and includes the 27 bp perfect palindrome and the AT-rich sequence but not the early element of the SV40 origin region (10). Double-stranded DNA (dsDNA) substrates were obtained by annealing ssDNA(GAPDH) and ssDNA(Site2) to their respective complementary ssDNA strands (GAPDHrev 5′-ATA CGA CTC ACT ATA GGG CTC GGC TGG CGA CGC AAA AGA AGA TGC GGC TGA CTG TCG-3′ and SV40rev 5′-ATG GCT GAC TAA TTT TTT TTA TTT ATG CAG AGG CCG AGG CCG CCT CGG CCT CTG AGC-3′) following standard procedures (63). In addition, five oligonucleotides of different lengths that consisted exclusively of dT: $Oligo(dT))_{20}$, $Oligo(dT)_{30}$, $Oligo(dT)_{40}$, $Oligo(dT)_{50}$, and $Oligo(dT)_{60}$. All oligonucleotides were obtained from Sigma.

For EMSA experiments, oligonucleotides (the oligo(dT) substrates, ssDNA(GAPDH), and ssDNA(Site2) were radioactively 5′-end-labelled using T4 polynucleotide kinase (New England Biolabs (NEB)) following the manufacture's procedure. The labeling was done in a 20 μl reaction volume consisting of T4 polynucleotide kinase reaction buffer, 2.5 μCi/μl [γ-^{32}P]-ATP (3000 Ci/mmol, Perkin Elmer), and 1 U of polynucleotide kinase (NEB) at 37°C for 10 min. The labelled oligonucleotide was purified using GE Healthcare spin columns. For EMSA experiments on dsDNA substrates, the radioactive oligonucleotides (above) were annealed to their complementary sequences and purified.

For atomic force microscopy (AFM) experiments, several hundred base pairs (bp) long DNA substrates that contained an ssDNA region at ∼50% of the DNA fragment length were prepared, similar as described (64). The ssDNA stretch has a length of 48 nt (5′-GGT CGA CTC TAG AGG ATC AGA TCT GGT ACC TCT AGA CTC GAG GCA TGC-3′, ssDNA (gap) as described in Supplemental Table S1). For the preparation, a modified plasmid, pUC19N (2729 bp) containing two restriction sites of the nickase Nt.BstNBI (New England Biolabs, NEB) at a distance of 48 nt was first incubated with Nt.BstNBI for a total of 2.5 h at 55°C. The short 48 nt ssDNA stretch between the nicks was then removed by repeated (8 times) heating to 68°C for 20 min at 300 rpm in the presence of a ∼20-fold excess of counter oligonucleotide followed by spin filtering using a 0.5 ml 50 kD MWCO spin filter (corresponding to a ssDNA cut off of 125 nucleotides (nt) and a dsDNA cutoff of 100 bp; Amicon Ultra). To obtain the long DNA substrate with a 48 nt ssDNA (gapped) region (8.8% of total DNA substrate length) at 49.0% of the DNA length (547 bp

– 48 nt), the plasmid was finally digested using the restriction enzymes BspQI and NdeI (NEB). The DNA substrate was purified by gel electrophoresis with a 1% agarose gel followed by gel extraction using the Nucleo Spin Gel and PCR Clean-up kit (Macherey Nagel).

In analytical ultracentrifugation (AUC) experiments, 48 nt long oligonucleotide of the same sequence as the ssDNA stretch of the DNA substrate for AFM (above) was obtained from Sigma. All oligonucleotide sequences used are listed in Supplemental Table S1.

Differential scanning fluorimetry (DSF)

Differential scanning fluorimetry (DSF) provides a method to study protein stability in dependence of interacting factors by analyzing the melting temperatures of a protein in the absence and presence of co-factors and interaction partners, which yields insights in their physical interactions with the protein (65). The physical interactions of SV40 Tag with ssDNA and dsDNA, in the presence and absence of 1 mM ATP and 5 mM MgAc were evaluated by DSF as previously described (66,67). Briefly, the assays were performed using 1× fluorescent dye Sypro Orange (Applied Biosystems) in 30 mM HEPES–KOH, pH 7.8, 150 mM NaCl, with SV40 Tag set at a fixed concentration of 1 μM and titrations of DNA. The ssDNA and dsDNA substrates used in these experiments are listed in Supplemental Table S1. The samples were transferred to 96-well Fast Thermal Cycling Plates (Applied Biosystems) and subjected to a heating ramp of 1.0°C per min from 25 to 90°C with fluorescence intensity readings at 470 nm excitation and 550 nm emission wavelengths using a StepOnePlus System (Applied Biosystems). The obtained data were analyzed using Protein Thermal Shift Software v1.1 (Applied Biosystems) and GraphPad Prism 5 software (GraphPad) as described previously (66,67). All experiments were carried out at least in triplicate.

Electric mobility shift assay (EMSA)

Radioactively labelled oligonucleotides were incubated at the indicated concentrations of protein in HEPES binding buffer (10 mM HEPES–KOH, pH 7.8, 1 mM EDTA and 40 mM NaCl) for 30 min in a volume of 15 μl as previously described (62). Then 6× loading buffer (Thermo Fisher Scientific) was added and the protein-nucleic acid complexes were analyzed in an electro-mobility shift assay (EMSA) using a 7% native polyacrylamide gel in 0.5× TBE. The running conditions were 70 V for 60 min using 0.5× TBE as electrode buffer until bromophenol blue dye was run two-thirds of the way through the gel. The gel was transferred to Whatman 3MM paper, wrapped in cling film and exposed overnight to imager screens (Fujifilm) using a FLA5100 phosphoimager (Fujifilm) for autoradiography detection. Multi Gauge Image Analyzer (Fujifilm) was used to determine bands intensity and the resulting data were analyzed using non-linear least-square fitting with GraphPad Prism 5 software (GraphPad). All reported K_D values were determined from at least three independent experiments.

Native polyacrylamide gel electrophoresis (PAGE)

SV40 Tag with or without DNA (ssDNA or dsDNA as indicated), 1 mM ATP and/or 5 mM MgAc in 30 mM HEPES–KOH, pH 7.8, 150 mM NaCl was incubated for 10 min at 37°C. The samples were mixed with 6x non-reducing sample buffer (600 mM Tris–HCl, pH 7.8, 50% glycerol, 0.02% bromophenol blue) and loaded onto a precast 4–15% Tris glycine native gel (Biorad). The gel was run in Tris-glycine buffer at 150 V for 60 min and stained with Coomassie Brilliant blue R-250 (Thermo Fisher Scientific). For western blot, the gel was transferred onto a methanol-activated PVDF membrane using G2 fast blotter (both Thermo Fisher Scientific) according to manufacturer's instructions. After blocking, the membrane was probed with SV40 Tag polyclonal primary antiserum R15 (1:10 000) (kindly provided by W. Deppert; (68,69)) and peroxidase-conjugated donkey anti-rabbit secondary antibody (1:10 000) (Jackson Labs) and the bands were visualized using West Pico Chemiluminescent Substrate Super Signal (Thermo Fisher Scientific) according to manufacturer's instructions.

Analytical ultracentrifugation (AUC)

Analytical ultracentrifugation (AUC) sedimentation velocity (SV) runs were performed at 40 000 rpm and 20°C using a Proteomelab XL-I AUC (Beckman Coulter) with an 8-hole 50Ti rotor (Beckmann Coulter). 400 μl of samples plus reference buffer (25 mM HEPES–NaOH, pH 7.5, 25 mM sodium acetate, 10 mM magnesium acetate) were filled in 2-channel Epon cells with an optical path length of 12 mm and sapphire windows (Beckmann Coulter). T antigen was applied at a concentration of 1, 2.5 or 5 μM as indicated. If present, ATP was applied at 50 μM and ssDNA at 500 nM. As control, 500 nM ssDNA were also applied alone (in the absence of protein). The data were collected using absorption optical detection at a wavelength of 280 nm. Sufficient scans to capture complete sedimentation were analyzed using the software Sedfit (version 12.52) to obtain a sedimentation coefficient distribution $c(s)$ from the Lamm equation with a confidence interval of 0.68, as described (70).

Atomic force microscopy (AFM)

To study DNA binding of SV40 Tag by AFM, the protein was incubated at concentrations of 50 or 500 nM with the ∼500 bp gapped DNA substrate (3–5 nM; see above) in the absence or presence of 1 mM ATP for 1 h at room temperature (RT). $Tag_{131–627}$ shortened construct (wild type and the monomeric V350E/P417D variant) was incubated at 500 nM with the gapped DNA substrate in the presence of ATP as for the full length wild-type Tag. All incubations were carried out in AFM buffer (25 mM HEPES–NaOH, pH 7.5, 25 mM sodium acetate, and 10 mM magnesium acetate). To study RPA interactions with SV40 Tag and ssDNA, samples were incubated as in the absence of RPA, with addition of 10 nM RPA in the reaction mixtures. Monomeric $Tag_{131–627}$ (V350E/P417D) was incubated with RPA and DNA substrate under identical conditions. As a control, RPA (10 nM) was also incubated with the gapped DNA substrate in the absence of Tag (1 h incubation at RT in 1 mM ATP

containing AFM buffer). To confirm the presence and stoichiometry of RPA in the ssDNA bound complexes, incubations were repeated for Tag (500 nM) and RPA (10 nM) samples in the presence of ATP with additional incubation with an RPA antibody (10 nM, Abcam) for 20 min. Following incubation, all samples were crosslinked with 0.1% glutaraldehyde for 10 min at RT. 20 μl of sample solution were then immediately deposited onto freshly cleaved mica (SPI supplies), rinsed with filtered, deionized water, and dried in a gentle stream of nitrogen. As negative control, the DNA substrate was also imaged alone (in the absence of protein) at a concentration of 4 nM. All experiments were carried out at least in duplicate.

To study the oligomerization of Tag in the absence of DNA, the protein was incubated at 500 nM in the presence of 1 mM ATP, at RT for 1 h or at 37°C for 10 min followed by crosslinking with 0.1% glutaraldehyde for 10 min at RT. Protein in the absence of DNA was diluted 2–20× for deposition onto mica in AFM buffer to reduce particle density in the sample.

All AFM images were recorded in air with a Molecular Force Probe (MFP) 3D AFM (Asylum Research) in oscillation mode using OMCL-AC240TS silicon probes (Olympus) with spring constants of ∼2 N m^{-1} and resonance frequencies of ∼70 kHz. AFM images were collected at a scan speed of 2.5 μm/s, image sizes of 1 × 1 μm^2 to 8 × 8 μm^2 and pixel resolutions of 1.95 nm/pixel. For analysis, AFM images were plane fitted and flattened to third order with the Igor Pro based MFP software (Asylum Research). Protein-DNA complexes were analyzed in terms of binding specificity for ssDNA within the dsDNA DNA substrate and volumes of the bound peaks, as previously described (71–74).

To determine binding specificity of Tag for ssDNA, initially the DNA lengths were measured with the freehand tool of the software Image J (NIH open-source software) by following the DNA backbone. DNA length distributions showed a major species with ∼150 nm. This length is consistent with 499 bp DNA (547 bp – 48 nt stretch, with a theoretical length of 170 nm using 0.34 nm/bp) assuming shortening due to unresolved DNA backbone undulations. Only DNA fragments with lengths within two standard deviations (SD) of the center of a Gaussian fit to the DNA lengths distribution were included in further analysis. Protein peak positions were measured as the distance from the peak center to the closer DNA end and are given as fraction of total DNA fragment length (distance from end divided by the full DNA length). Position distribution histograms were obtained using Origin Pro 8.6. In the histograms, 0% of DNA length corresponds to protein binding to the DNA fragment ends and 50% of DNA length corresponds to protein peaks bound to the middle of the DNA fragment (i.e. the position of the ssDNA). For calculating the specificity of SV40 Tag binding to the ssDNA, the end bound complexes were excluded by starting histograms at 2% of DNA length. Binding specificity for ssDNA results in a peak at 50% of DNA length (position of ssDNA gap), which was fit by a Gaussian curve. Binding specificity of SV40 Tag for ssDNA is obtained from the ratio of the integrated area under the Gaussian (A_{spec}) and the area of nonspecific binding background (A_{nsp}) on which the Gaussian is footed. A_{nsp} is calculated as the product of the background height (y_0) and the DNA length that is taken into account for the fits (48%). Together with the number of binding sites $N = 525$ (excluding 2 × 2% of DNA fragment length), the specificity (S) is defined as (74): $S = (A_{spec}/A_{nsp}) \times N + 1$.

The volumes of the protein-DNA complexes located at 50 ± 4% (SD) were measured using the software Image SXM, and statistically analyzed and plotted using Origin software. AFM volumes of dominant species were obtained as the centres of Gaussian fits to the statistical volume distributions (±1 SD from Gaussian widths). These volumes (V) were translated into protein molecular weight (MW) using a linear relationship: $MW = (V + 5.9)/1.2$, based on prior calibration of the AFM system using proteins with known MW (73). Volumes of protein peaks in the absence of DNA were measured and analyzed analogous to those on DNA.

DNA polymerase α-primase activity on ssDNA

The Pol-prim assay measures primase-initiated DNA synthesis on unprimed Φ174 ssDNA as previously described using SV40 DNA replication conditions (36,57) with slight modifications. In short, 40 μl of assay Tag samples (full length protein or shortened monomer variants as indicated) were incubated in buffer containing 30 mM HEPES–KOH, pH 7.8, 7 mM MgAc, 0.1 mM EGTA, 1 mM DTT, 0.25 mg/ml BSA, 0.01 mg/ml creatine kinase, 40 mM creatine phosphate, 4 mM ATP, 0.2 mM each of CTP, GTP and UTP, 100 μM of each dATP, dGTP and dTTP plus 50 μM dCTP in the presence of 0.1 μCi P32 α-dCTP (3000 Ci/mmol, Perkin Elmer) and 250 ng Φ174-ssDNA template (0.76 nmol nucleotides, NEB). Incubations were carried out in the absence or presence of RPA (0.5 μg, unless otherwise stated). The amounts of full length Tag and variant proteins in the reactions are indicated individually. The reaction mixture was assembled on ice, and the reaction was started by the addition of 10 ng of human Pol-prim. After incubation for 1 h at 37°C, the reaction was spotted on Whatman GF-C glass fiber filters and submerged in 10% trichloroacetic acid as previously described to measure the amount of incorporated nucleotides (57,58).

RESULTS

High affinity binding of SV40 T antigen to single-stranded DNA sequences

The ability of SV40 T antigen (Tag) to bind to ssDNAs was examined using differential scanning fluorimetry (DSF) and electromobility shift assays (EMSAs). DSF and EMSA experiments provide highly complementary insights into protein interactions. The interactions of proteins with ligands, cofactors and substrates in many cases stabilize protein structure and increase the melting temperature of the protein (75). DSF investigates protein stability in dependence of interacting factors (such as DNA or ATP) by measuring the melting temperature of the protein in the absence and presence of different factors (65). In contrast, DNA gel shift assays separate and visualize distinct protein-DNA complexes (76). Our results show that SV40 Tag binds ssDNA with high affinity both in solution as determined by DSF analysis and in the gel matrix of EMSA experiments.

ssDNA substrates (see Supplemental Table S1) were designed using naturally occurring sequences derived from human GAPDH cDNA (nonspecific ssDNA(GAPDH)) and SV40 recognition Site 2 (specific ssDNA(Site2)). Both ssDNA sequences have the same length (57 nucleotides) but they differ in their base composition and sequence. In particular, ssDNA(Site2) contains a specific target site sequence of Tag. Using DSF, we find that Tag efficiently interacts with non-specific and specific (Site2) ssDNA with K_D values of approximately 30 and 40 nM, respectively, in the absence of divalent cations and ATP (Figure 1A and B, summarized in Table 1). EMSA experiments performed in parallel also show high affinity binding with K_D values in the range of 40 to 120 nM for SV40 Tag interacting with these ssDNA substrates in the absence of ATP and divalent cations (see below and Figure 1C–H as well as Table 1). Our results hence show that SV40 Tag binds to ssDNA with an apparent affinity in the range of 30–120 nM independent of DNA sequence or base composition as determined by DSF and ssDNA gel shift assays.

High and low mobility complexes of SV40 T antigen with single-stranded DNA sequences

Stable hexameric Tag complexes have been reported in the presence of ATP both on dsDNA and ssDNA as well as in the absence of DNA *in vitro* using various techniques (19,20,44,47,52,77–79). Moreover, SV40 Tag has previously been extracted from cells (*in vivo*) in a hexameric form at intermediate and high protein concentrations when the protein was purified under native conditions without harsh pH shift settings, similar to the way SV40 Tag was purified here (47,80,81). Our EMSA data clearly differentiate two different molecular weight complexes of Tag with ssDNA (Figure 1C and D), a very slow-moving complex (Complex 1) and a faster-moving complex (Complex 2). The large, oligomeric protein–DNA complex, Complex 1, likely represents hexameric Tag bound to ssDNA (52), whereas Complex 2 most likely consists of monomeric Tag bound to these ssDNA sequences (see detailed structural analyses below). In our experiments, the two different 57-mer ssDNAs were bound by Tag with similar efficiencies of forming oligomeric Complex 1 depending only slightly on the oligonucleotide sequence. Specifically, K_D values of ∼40 and ∼80 nM were determined for Complex 1 formation using ssDNA(Site2) and ssDNAs(GAPDH) substrate, respectively (Table 1). Interestingly, the affinities of Tag for ssDNA were only slightly lower for the fast moving, likely monomeric Tag-containing Complex 2 than for the slow-moving, oligomeric Tag-containing Complex 1. From the EMSA data, K_D values for the formation of the fast migrating Complex 2 were determined as ∼60 and ∼120 nM for binding of Tag to Site 2 and GAPDH ssDNAs, respectively (Figure 1, panels C and D, Table 1). These results show that Tag interacts very efficiently and sequence independently with ssDNA both as a monomer and oligomer/hexamer.

To evaluate if monomeric Tag protein on DNA may be a consequence of oligomeric complex disruption by the gel matrix of native PAGE, crosslinking of these complexes prior to gel analyses was carried out. In the case of Tag binding to ssDNA(GAPDH), crosslinking had only minor influences on the formation of the two complexes and both complexes could be readily detected (Figure 1E and F). Quantification of experiments revealed that the apparent affinity of Tag for ssDNA(GAPDH) to form the Tag-ssDNA(GAPDH) Complex 1 (oligomeric Tag) was slightly decreased after crosslinking (K_D ∼110 nM). Furthermore, the fast migrating Complex 2 (monomeric Tag) was also clearly detectable (K_D ∼120 nM). In contrast, on ssDNA containing the SV40 Tag recognition sequence site 2 (ssDNA(Site2)) the oligomeric Tag-containing Complex 1 was detected as the exclusive species of T antigen binding after incubation with crosslinking agent whereas the monomeric Tag-ssDNA complex species, Complex 2, was absent under these experimental conditions (compare Figure 1G and H). The overall affinity of Tag binding to ssDNA(Site2) was not altered and comparable to in the absence of crosslinking, with a K_D value of ∼70 nM.

In summary, these experiments suggest that Tag binds ssDNA very efficiently and depending on the sequence environment two complexes (a fast and a slow migrating complex) or one complex, the slow migrating large, hexameric/double-hexameric complex can be found using EMSA gels. The differences in the complex formations of Tag with these ssDNAs can be explained at least in part by considering that ssDNA(Site2) contains the '27 bp perfect palindrome' of the SV40 origin region (10). Short stable hairpin formation of this sequence (containing two SV40 Tag recognition sites GAGGC and flanking ssDNA stretches) may stabilise hexameric and double-hexameric complexes in solution but not sufficiently to survive the native PAGE step of an EMSA without crosslinking. In contrast, ssDNA(GAPDH) does not form stable secondary structures according to structure predictions (data not shown) and two Tag-ssDNA complexes (likely hexameric/double-hexameric and monomeric) have been determined with and without crosslinking prior to PAGE (see Figure 1E and F).

Binding of SV40 T antigen to double-stranded DNA sequences

The interaction of Tag with dsDNA is well characterized, in particular its binding to the so called sites 1 and 2 of the non-coding control region NCCR (17,18,46,51). DSF and EMSA experiments were used to investigate Tag binding to dsDNA, dsDNA(Site2) and dsDNA(GAPDH) (Figure 2; see Table 2 and Supplemental Table S1), and to directly compare it to ssDNA binding (Table 1).

Our DSF results show that Tag interacts only very weakly with dsDNA lacking a specific Tag-binding site such as dsDNA(GAPDH). We determined a K_D value of 5800 ± 4000 nM for binding to dsDNA(GAPDH) (Figure 2A and Table 2). As expected Tag has a higher affinity for dsDNA(Site2), which contains the Tag-binding site 2 (K_D value 120 ± 110 nM, Figure 2B and Table 2). These results clearly confirm sequence specificity in dsDNA binding of Tag and are in agreement with previous publications that report inefficient binding of Tag to dsDNA lacking a Tag binding site (44,46,48). Notably, the affinity of Tag to dsDNA containing site 2 was lower than Tag's affinity for ssDNAs using the

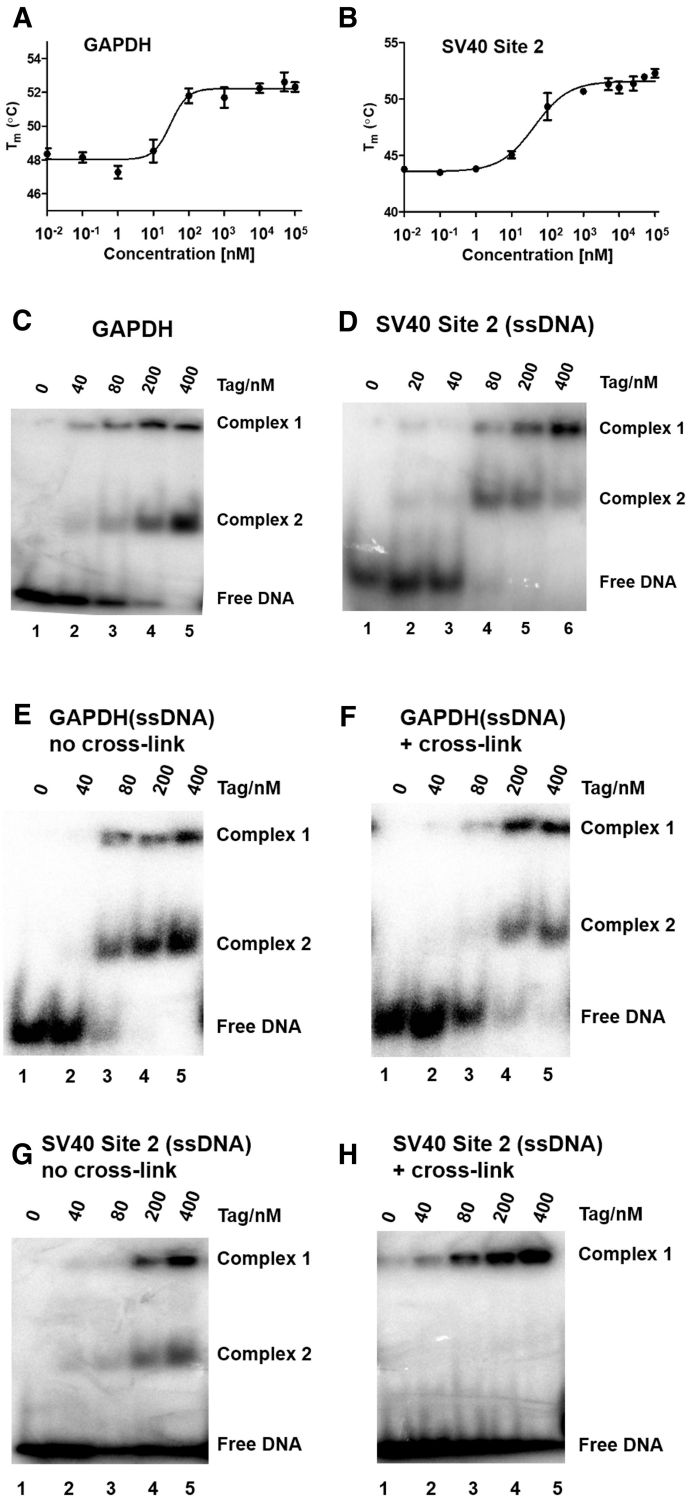

Figure 1. Binding of SV40 Tag to ssDNA. (A, B) Interaction of SV40 Tag with nonspecific GAPDH ssDNA (**A**) and Tag recognition site 2-containing ssDNA (**B**) measured by DSF. The experiments were performed using SV40 Tag set at a fixed concentration of 1 μM and titrations of GAPDH ssDNA (A) or SV40 site 2-containing ssDNA (B) in 30 mM HEPES–KOH, pH 7.8, 150 mM NaCl and 1x fluorescent dye Sypro Orange. The samples were subjected to a gradient increase in temperature from 25 to 90°C and the melting temperature of Tag for each DNA concentration was determined using Protein Thermal Shift software v1.1 (Applied Biosystems) and the resulting data were further analyzed with Graph pad prism software (GraphPad). Experiments were carried out in triplicates and the mean of the melting temperature and the standard deviation are presented. (C, D) EMSA analyses of SV40 Tag binding to ssDNA. Increasing concentrations (40, 80, 200 and 400 nM; lanes 2–5) of Tag were incubated with 10 fmol of radioactively labeled ssDNA with GAPDH sequence (**C**) or site 2-containing sequence (**D**). For comparison, the gel shift of each DNA sample was also analyzed in the presence of only assay buffer (lane 1). (**E–H**) Tag at the indicated concentrations was incubated with GAPDH ssDNA in the absence (E) or presence of crosslinker (F) and with site 2 containing ssDNA in the absence (G) or presence of crosslinker (H). Glutaraldehyde at 0.1% was used for crosslinking.

Table 1. KD values of Tag interacting with ssDNA 57mer

	SV40 Large T antigen binding to			
	ssDNA w/o MgAc & ATP	ssDNA with MgAc (5 mM)	ssDNA with ATP (1 mM)	ssDNA with MgAc (5 mM) and ATP (1 mM)
Conditions	KD (nM)	KD (nM)	KD (nM)	KD (nM)
DSF				
GAPDH	30 ± 10	10 ± 1	100 ± 20	1,500 ± 1100
Site 2 (DSF)	40 ± 7	50 ± 10	100 ± 30	200 ± 60
EMSA				
GAPDH (1)	80 ± 40	30 ± 10	160 ± 40	40 ± 10
GAPDH (2)	120 ± 20	50 ± 10	170 ± 30	140 ± 70
Site 2 (1)	40 ± 5	20 ± 6	80 ± 30	70 ± 8
Site 2 (2)	60 ± 9	60 ± 4	170 ± 50	65 ± 10
Site 2 (1)*	70 ± 10*	40 ± 10*	160 ± 60*	130 ± 60*

(1) EMSA complex 1; (2) EMSA complex 2; * determined after crosslinking of products.

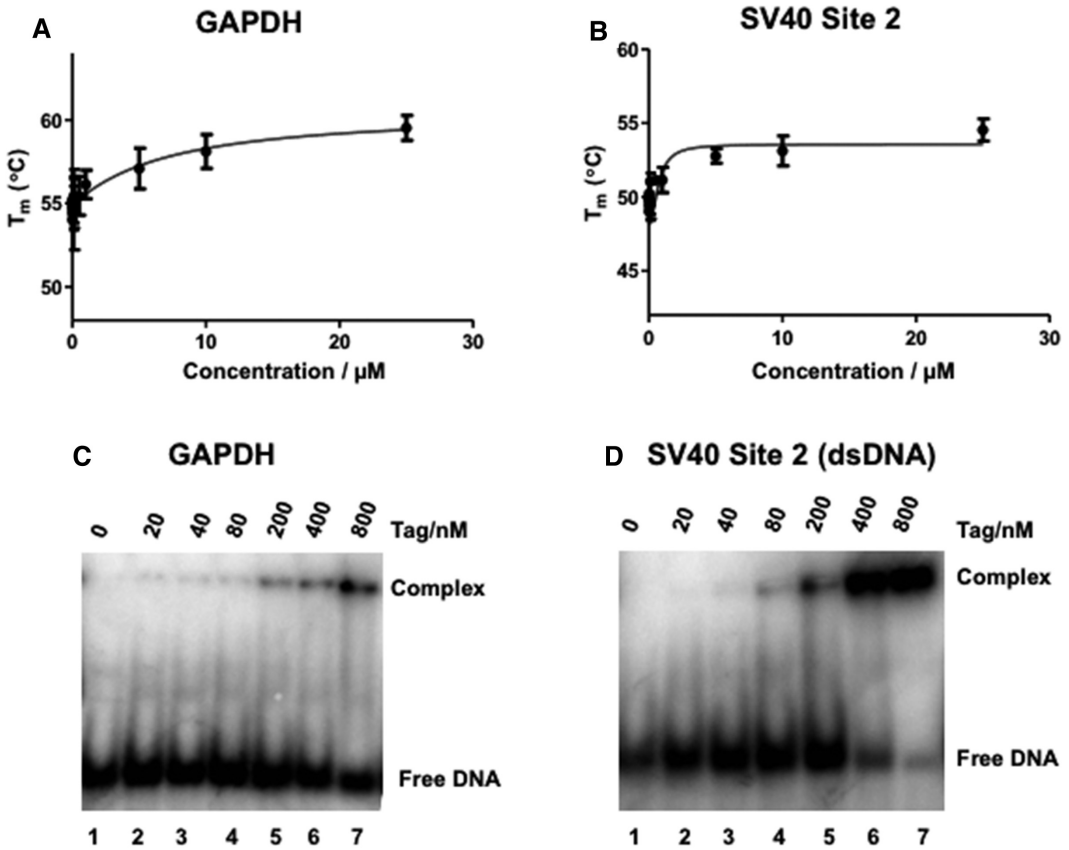

Figure 2. Binding of SV40 Tag to dsDNA. (A, B) Interaction of SV40 Tag with nonspecific GAPDH dsDNA (**A**) and Tag recognition Site 2 dsDNA (**B**) measured by DSF. The experiments were performed using SV40 Tag set at a fixed concentration of 1 μM and titrations of GAPDH dsDNA or SV40 site 2-containing dsDNA as in Figure 1 for ssDNA. (C, D) EMSA analyses of SV40 Tag (20, 40, 80, 200, 400, and 800 nM; lanes 2–7) incubated with 10 fmol of radioactively labeled nonspecific dsDNA (GAPDH sequence, **C**) or SV40 site 2-containing sequence (**D**). For comparison, the gel shift of each DNA sample was also analyzed in the presence of only assay buffer (lane 1). Experiments were carried out as in Figure 1.

same assay conditions (compare Figure 1B and 2B; see also Tables 1 and 2).

We also observed lower affinities of Tag for dsDNA than for ssDNA in EMSA experiments (Figure 2C and D compare to Figure 1C and D). Consistent with our DSF data and with previous reports (44,46,48), the interaction of Tag with dsDNA containing the SV40 binding site 2 was significantly more efficient than with non-specific ds-DNA(GAPDH), with apparent K_D values of ∼100 nM for dsDNA(Site2) and >>1000 nM for the non-specific ds-DNA (see Table 2). In contrast to EMSAs with ssDNA, the Tag–dsDNA complexes only showed a single slow-moving species (oligomeric Tag) in native PAGE. These data strongly suggest that Tag interacts with dsDNA exclusively in a higher order oligomeric, likely hexameric or double-hexameric form, as previously reported (18,51,52).

Table 2. KD values Tag binding to dsDNA

	SV40 large T antigen binding to	
	dsDNA w/o MgAc/ATP	dsDNA with MgAc (5 mM) and ATP (1 mM)
Conditions	K_D (nM)	K_D (nM)
DSF		
GAPDH	5800±4000	600±340
Site 2	120±110	160±40
EMSA		
GAPDH (1)	>>1000	>>1000
Site 2 (1)	100±50	220±130

(1) EMSA Complex 1.

Interestingly, binding of Tag to neither of the dsDNA substrates was influenced by crosslinking with glutaraldehyde in EMSA experiments (data not shown). It is important to note that the affinities to double stranded oligonucleotides described here for the full length protein using DSF and EMSA are slightly lower than those reported earlier for T antigen deletion mutants OBD (aa131 to 260) and N260 (aa 1–260) (45,48). This difference could be explained by the use of different oligonucleotide sequences, the expression and purification and thus modification of the proteins (full length Tag expressed in insect cells versus deletion mutants of Tag expressed in *E. coli*), or the experimental set up using DSF and EMSA versus fluorescence anisotropy (48,67). It is worth to mention that by using the insect cell-expressed SV40 Tag Fradet-Turcotte *et al.* (2007) found apparent K_D values of 170±22 nM for specific and 494±38 nM for unspecific double-stranded oligonucleotides in the presence of ATP, which is comparable to our results of 160±40 and 600±340 nM, respectively ((48) and Table 2).

Stimulated formation and stabilization of Tag hexamers by ATP and ssDNA

To study the effects of ATP and DNA on Tag oligomerization and stability, we employed DSF, EMSA, and analytical ultracentrifugation (AUC). ATP binding has been previously shown to support Tag oligomerization in the absence of DNA (82) and on dsDNA replication origin regions (44,83). We incubated Tag protein with ATP, Mg^{2+}, ssDNA, dsDNA, or combinations thereof, and its melting temperature and thus stability was measured by DSF. Our DSF results show that all of these cofactors and substrates of Tag individually increased the melting temperature of the protein (Figure 3A and Supplemental Figure S2). In addition, the combination of ATP, Mg^{2+} and ssDNA or dsDNA increased the Tag melting temperature and hence stability further (Figure 3A and Supplemental Figure S2). The respective melting temperatures are summarized in Supplemental Table S2. These data indicate stabilization of Tag *via* interactions with Mg^{2+}, ATP, ssDNA, or dsDNA, likely due to different conformational properties of Tag protein and complexes under the different conditions. In addition, PAGE was performed with Tag in the absence and presence of Mg^{2+}, ATP, and/or ssDNA under non-denaturing conditions (Figure 3B and Supplemental Figure S3). The native PAGE data show higher order oligomers in solution at Tag concentrations ≥500 nM (Figure 3B and Supplemental Figure S3). Our results further show that the addition of ssDNA stimulates the formation of oligomeric SV40 Tag complexes, with ATP contributing further to this stimulation (Figure 3B, compare lane 4 and 5).

Furthermore, we corroborated oligomerization of Tag in solution in the presence of ssDNA and/or ATP/Mg^{2+} by analytical ultracentrifugation (AUC, Figure 3C). Sedimentation coefficients of 4–6 S for monomeric and 14–17 S for hexameric SV40 Tag have previously been reported (18,20,47). Our AUC data show that at 5 μM of protein, in addition to a ∼4 S species (grey arrow in Figure 3C), in the absence of co-factors a sparsely populated higher molecular weight complex is present in our recombinant SV40 Tag samples with an approximate sedimentation coefficient of ∼13 S (dashed line in Figure 3C). Addition of 500 nM ssDNA (without ATP) clearly increased the formation of higher order molecular weight complexes in a concentration-dependent manner (light grey line in Figure 3C and Supplemental Figure S4). We interpret this complex species, which is characterized by a sedimentation coefficient of ∼15 S, as hexameric Tag complexes bound to ssDNA (Figure 3C, black arrow). Adding ATP (in the absence of ssDNA, dark gray line in Figure 3C) enhanced the formation of these presumably hexameric complexes to a similar degree as ssDNA did (see black arrow-marked complexes in Figure 3C). In particular, the joint action of ssDNA and ATP/Mg^{2+} resulted in a significant increase in hexamer formation (compare black line with grey lines in Figure 3C and Supplemental Figure S4 panels B and C)), consistent with our native PAGE analyses (Figure 3B).

In summary, these findings suggest that SV40 Tag monomers tend to interact with each other with low affinity to form higher molecular weight complexes in solution. Furthermore, the addition of ATP or ssDNA enhances complex formation and stabilizes hexameric forms in solution. Moreover, our data show that ssDNA and ATP cooperate to stabilize these large Tag complexes and that crosslinking of these complexes is not required to allow their detection by native PAGE or AUC (Figure 3B and C, respectively).

Effects of ATP on Tag–DNA interactions

Next, we investigated the effect of ATP and Mg^{2+} on Tag interactions with the short ssDNA and dsDNA sequences in more detail. DSF results show that the addition of Mg^{2+} alone did not significantly change the affinity of Tag to the ssDNA substrates. K_D values of 10 nM and 50 nM for ssDNAs(GAPDH) and ssDNA(Site2) substrate, respectively, were found (Table 1). Interestingly, the presence of 1 mM ATP in the binding buffer decreased the affinity of Tag to both ssDNA substrates, with an apparent K_D of about 2- to 3-fold higher than in the absence of ATP (K_D ∼100 nM in the presence of ATP versus 30 and 40 nM in the absence of ATP obtained by DSF, Table 1). The presence of 1 mM ATP and 5 mM Mg^{2+} together reduced the apparent affinity of Tag for the two employed ssDNA sequences further (K_D values of ∼200 nM and ∼1.5 μM

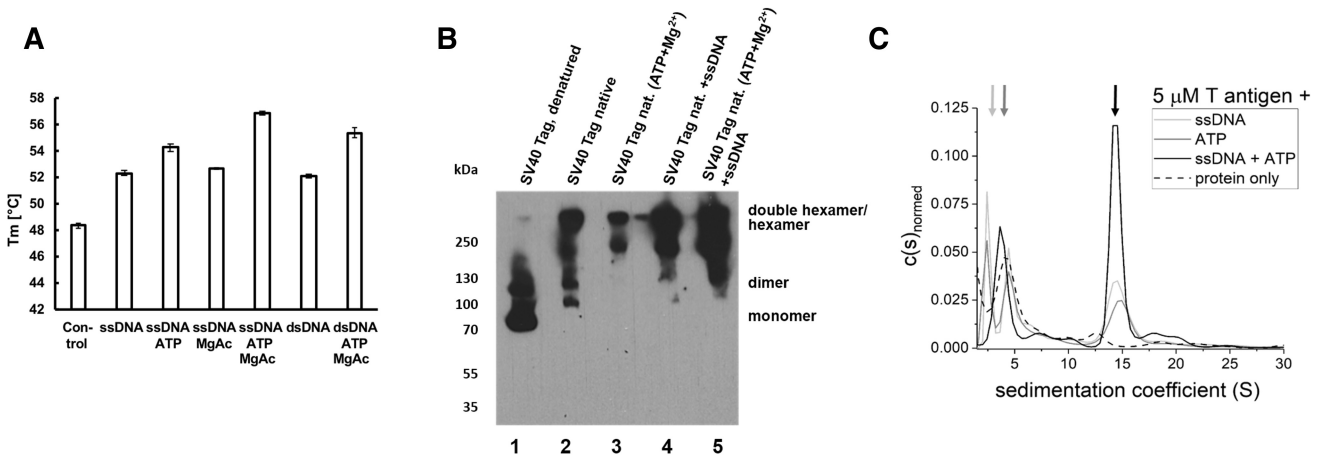

Figure 3. Effect of DNA, ATP and Mg^{2+} on SV40 Tag protein stability and molecular complex formation. (**A**) SV40 Tag protein stability in the presence of ssDNA or dsDNA with or without ATP and Mg^{2+} was analyzed using DSF. The experiments were performed using 1 μM SV40 Tag plus 50 μM ssDNA or dsDNA with or without 1 mM ATP and 5 mM MgAc, as indicated, in 30 mM HEPES–KOH, pH 7.8, 150 mM NaCl with 1× fluorescent dye Sypro Orange. (**B**) SV40 Tag complex formation in presence of ssDNA, ATP and Mg^{2+}. Lanes 2 to 4: 500 nM of SV40 Tag with or without ssDNA, ATP and Mg^{2+} were incubated in 30 mM HEPES-KOH, pH 7.8, 150 mM NaCl. Lane 1: 100 nM of SDS-denatured SV40 Tag, Lane 2: SV40 Tag, Lane 3: SV40 Tag with ATP and Mg^{2+}, Lane 4: SV40 Tag with ssDNA (200 nM ssDNA(Site2)), Lane 5: SV40 Tag with ssDNA, ATP and Mg^{2+}. Proteins and protein–DNA complexes were separated by native PAGE using a 4–15% Tris–glycine gel. The western blot was performed using polyclonal primary antibody recognising SV40 Tag (1:10 000) and peroxidase-conjugated donkey anti-rabbit secondary antibody (1:10000). (**C**) AUC sedimentation velocity experiments show that ATP binding enhances the stability of hexameric complexes of SV40 Tag on ssDNA (arrow, black curve) as well as intermediate (5–12 S) and higher (>15 S) oligomeric states. Incubations of Tag with either only ssDNA (light grey curve) or only ATP (dark gray curve) show comparable and significantly less hexamerization of Tag than in the presence of both ssDNA and ATP (black curve).

for ssDNA(Site2) and ssDNA(GAPDH), respectively, using DSF, see Table 1). To test whether decreased apparent binding affinity in the presence of ATP/Mg^{2+} was due to ATP hydrolysis driven translocation off the ssDNA, we repeated the DSF measurements with ssDNA in the presence of non-hydrolysable ATPγS. Surprisingly, the resulting K_D values indicated weaker rather than stronger apparent ssDNA binding by Tag in the presence of ATPγS compared to in the presence of ATP or in the absence of cofactor (K_D values of 300 nM for ATPγS and ∼40 μM for ATPγS and Mg^{2+} for both Site2 and GAPDH ssDNA, data not shown). These data suggest that ATP binding may either hinder ssDNA binding by Tag or induce and stabilize Tag hexamer assembly on ssDNA, which can slide off short ssDNA substrates in an ATP hydrolysis independent manner.

In contrast to ssDNA, binding of Tag to dsDNA substrates was stimulated by the presence of ATP/Mg^{2+} in DSF experiments. K_D values of 5.8 μM and 600 nM were obtained for non-specific dsDNA in the absence and presence of ATP/Mg^{2+}, respectively. In agreement with previous reports (43,44), the binding of Tag to dsDNA(Site2) was consistently stronger than binding to non-specific dsDNA(GAPDH) under these conditions. However, the specificity for its target sequence was slightly reduced in the presence of ATP/ Mg^{2+} compared to in the absence of co-factor, due to enhanced non-specific background binding. Tag bound about 50 times more efficiently to site 2-containing dsDNA compared to non-specific dsDNA in the absence of ATP/Mg^{2+} (∼120 nM for dsDNA(Site2) versus ∼5.8 μM for dsDNA(GAPDH); Table 2), and only about 4-fold better to site 2-containing dsDNA than to non-specific dsDNA in the presence of ATP/Mg^{2+} (∼160 nM for dsDNA(Site2) *versus* ∼600 nM for dsDNA(GAPDH); Table 2).

In contrast to DSF, EMSA analyses showed no major effect of ATP and Mg^{2+} on Tag binding to the ssDNA oligonucleotides or to the double-stranded DNA substrates (Supplemental Figure S1 and data not shown, Tables 1 and 2). In the presence of ATP/Mg^{2+}, a K_D of ∼70 nM was determined for the specific ssDNA substrate (ssDNA(Site2), versus 40–60 nM in the absence of ATP). For the non-specific ssDNA substrate (ssDNA(GAPDH)), hexameric Tag complexes showed similar, but slightly enhanced binding in the presence compared to in the absence of ATP (40 nM *versus* 80 nM, respectively, Table 1 Complex 1). For the monomeric protein species and non-specific ssDNA, the K_D was comparable in the absence and presence of ATP (Table 1). In agreement with the DSF results, EMSA data displayed significantly more efficient binding of Tag to site 2-containing dsDNA than to non-specific dsDNA, in the absence as well as presence of ATP. The apparent K_D values for dsDNA(Site2) Tag-binding in the absence and presence of ATP were ∼100 and ∼220 nM, respectively (Figure 2C and D, Table 2). For non-specific dsDNA (dsDNA(GAPDH)), a K_D value could not be determined by EMSA but was estimated as $K_D >> 1000$ nM, similar as in the absence of ATP.

Structural characterization of monomeric and oligomeric Tag complexes on ssDNA

To resolve structural aspects of ssDNA binding and oligomerization by SV40 Tag, we applied atomic force microscopy (AFM) imaging to samples of 50 or 500 nM of Tag in the presence or absence of ATP/Mg^{2+} (1 mM/10 mM)

and/or DNA (3–5 nM) as indicated. The DNA substrate employed in these experiments contains a 48 nt ssDNA stretch located in the center flanked by dsDNA. Measuring the positions of the bound protein peaks along the long DNA substrates as their distances from the DNA fragment ends provides binding preferences to the ssDNA stretch as enhanced binding peaks at ∼50% of the DNA length (Figure 4). From the resulting position distributions, we calculate specificities (S) for ssDNA over dsDNA binding of $S > 1000$ in the presence of ATP/Mg^{2+} (meaning a more than 1000-fold preferential binding of Tag to ssDNA *versus* dsDNA, Figure 4A and 4B central panels; summarized in Supplemental Table S3). In the absence of ATP, we observe a considerably reduced specificity of Tag ($S \sim 270$, Figure 4C left and center, Supplemental Table S3). Our DSF data suggested lower rather than higher non-specific dsDNA background binding in the absence of ATP (see above and Table 2). Instead, reduced specificity of Tag in the absence of ATP may result from lower population of the hexameric Tag species with slightly higher affinity for non-specific ssDNA than monomeric Tag (Complexes 1 and 2 in Table 1, respectively).

To determine the oligomeric states of Tag–ssDNA complexes, we next pursued AFM volume analyses of protein peaks bound at the 48 nt ssDNA stretch (Figure 4 right panels). The AFM volume distributions show that at low Tag concentrations such as 50 nM, Tag binds to ssDNA as a monomer in the absence (data not shown) or presence of ATP (Figure 4A), with volumes of 76 ± 24 nm^3 corresponding to ∼70 ± 20 kDa (SV40 Tag M_r = 81.6 kDa). These volumes are slightly smaller than expected based on the molecular weight of Tag and our AFM volume calibration (73). They are, however, significantly larger than the volumes measured for ssDNA regions (at 50% of DNA length) in the absence of protein (∼60 nm^3, Supplemental Figure S5), likely corresponding to ssDNA superstructure or salt contaminations. At 500 nM Tag concentration in the absence of ATP (Figure 4C), Tag interacts with ssDNA also as a monomer (∼22%, 78 ± 23 nm^3) but also shows ∼35% of peaks with volume consistent with dimeric species (154 ± 30 nm^3), as well as oligomers with volumes between ∼200 and ∼500 nm^3, consistent with a range of intermediate states from monomer to maximally hexamer binding to ssDNA. The AFM volumes for 500 nM Tag in the presence of ATP but absence of DNA (Figure 4D) show a majority of particles (∼84%) consistent with a monomeric species (∼60 ± 35 nm^3) and 16% consistent with a Tag dimer (∼170 ± 35 nm^3). Consistent with our AUC results at higher protein concentrations, Tag oligomeric states observed by AFM were similar in the presence of ATP but absence of DNA, and in the presence of DNA but absence of ATP. In particular, ATP and ssDNA together strongly enhanced formation of higher order oligomeric complexes also in the AFM experiments (Figure 4B), with only ∼27% of particles consistent with monomeric Tag (91 ± 25 nm^3) and the majority consistent with higher order complexes. These higher oligomeric states include ∼40% particles with an average volume of ∼1300 nm^3, corresponding to ∼1100 kDa, consistent with a double-hexamer. Only ∼6% of peaks on the ssDNA showed volumes of ∼500 nm^3 (ca. 420 kDa), consistent with a single hexamer of Tag.

It is worth noting that in the AFM experiments, crosslinking of complexes with glutaraldehyde was employed as a precaution to prevent complex dissociation due to potential destabilization upon surface attachment. However, without crosslinking, higher order complexes consistent with double-hexameric volumes were still observed (Supplemental Figure S6), albeit at slightly lower frequencies and smaller volumes than observed in the crosslinked samples. These findings are consistent with our EMSA and AUC data that were obtained without crosslinking. It is also worth to note here that the double-hexameric complexes observed at 500 nM Tag by AFM are in apparent contrast to the dominant hexameric (not double-hexameric) species in AUC measurements at 5 μM Tag. These different oligomeric states may be a consequence of extremely different protein-to-DNA ratios employed in these different types of experiments; 10:1 in AUC versus ≥100:1 in AFM. Formation and stabilization of dimers of hexamers may also be supported by the DNA construct in AFM experiments, in which the ssDNA stretch is bordered at both its 5′ and 3′ end by a ss/dsDNA junction, possibly 'locking' protein complexes into the ssDNA gap.

Effects of ssDNA length on SV40 Tag–ssDNA complex formation

The estimation of the required binding site length on ssDNA is very important for the understanding of Tag–ssDNA interactions. Since we determined using DSF that SV40 Tag binds to poly(dT) with high affinity (Table 3) we analyzed the physical interaction of Tag with ssDNA substrates with lengths ranging from 20–60 bases using oligo(dT)-nucleotides to avoid sequence-specific effects (Figure 5 and data not shown; summarized in Table 3). EMSA assays were performed in the absence of ATP and showed that Tag bound very inefficiently to the two shortest oligonucleotides, $Oligo(dT)_{20}$ and $Oligo(dT)_{30}$, in these EMSA experiments (Figure 5A and data not shown). Even crosslinking the Tag-ssDNA complexes prior to subjecting them to PAGE did not enhance the detection of Tag binding to these two shortest oligo(dT) oligonucleotides (Figure 5A). At 1,600 nM Tag, less than 10% of the $Oligo(dT)_{30}$ ssDNA was shifted (Figure 5A, lane 9). In contrast, Tag bound ssDNA of ≥ 40 nt much more efficiently, with apparent K_D values of ∼30 nM for $Oligo(dT)_{40}$ (Figure 5B, Complex 2) and ∼10 nM for $Oligo(dT)_{50}$ ssDNA (Figure 5C, Complex 2). A similar K_D value was also determined for Tag interactions with $Oligo(dT)_{60}$ (see Table 3). The formations of protein-oligo(dT) complexes containing oligomeric Tag showed similar K_D values as measured for the monomeric Tag on $Oligo(dT)_{40}$ to $Oligo(dT)_{60}$. These data also confirm that the 48 nt ssDNA region within the long dsDNA substrate used in the AFM experiments and 48 nt ssDNA substrate used in the AUC studies (see above) constitute a sufficient length for efficient Tag binding. In summary, these data again confirm that Tag binds to ssDNA without sequence specificity, and suggest that the minimum length of

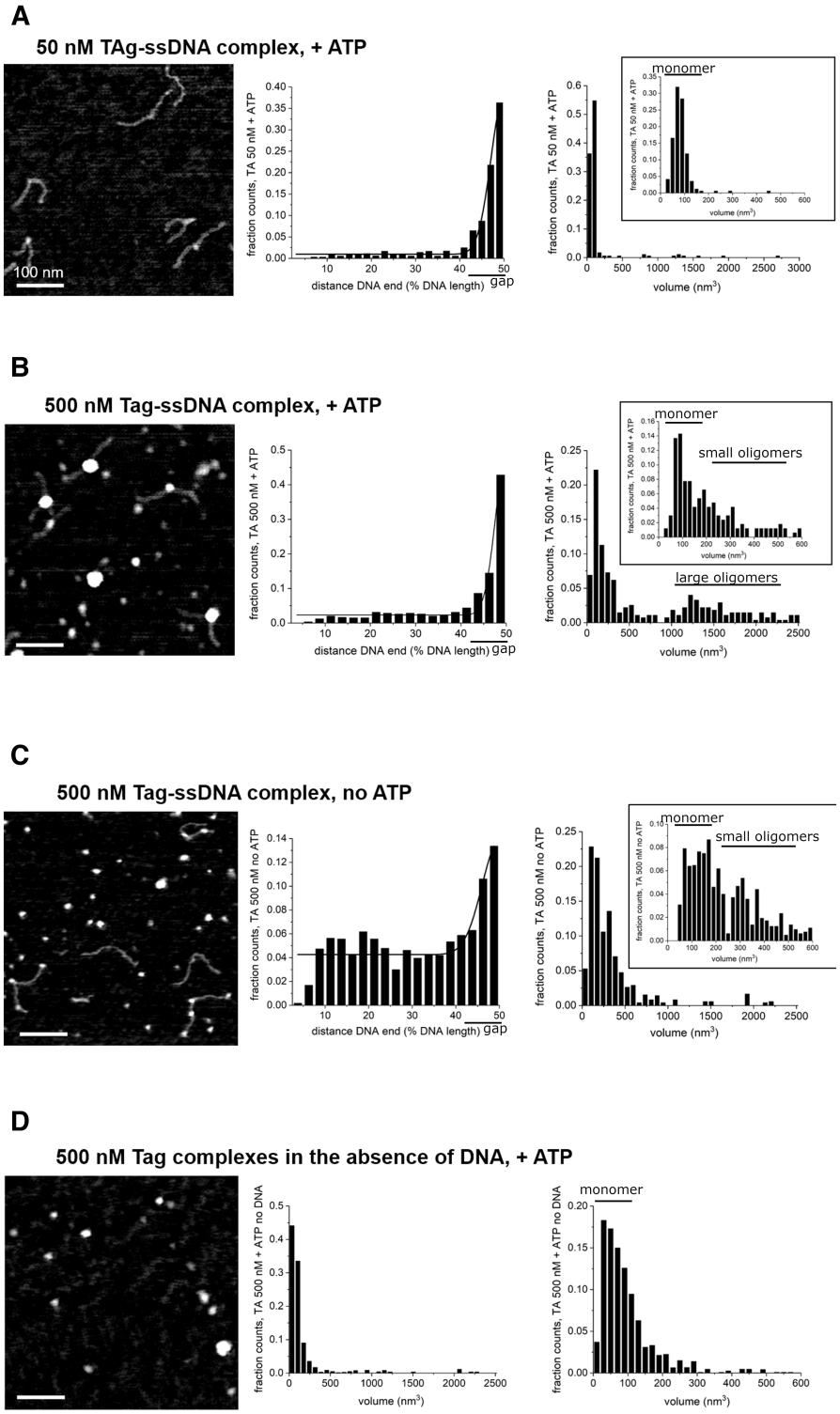

Figure 4. Increasing concentration, ATP binding, and DNA all support SV40 Tag oligomerisation. Atomic force microscopy (AFM) imaging plus quantifications of DNA substrate containing a central ssDNA region at 50% of the DNA length and (**A**) 50 nM Tag in the presence of ATP, (**B**) 500 nM Tag in the presence of ATP, and (**C**) 500 nM Tag in the absence of ATP. (**D**) 500 nM Tag in the presence of ATP but without ssDNA. Protein binding position distributions on the DNA substrate (A–C central panels**)** show strong binding preference for ssDNA region (position indicated on x-axis as 'gap') with Gaussian fit centres at 50% of DNA substrate (black lines) at low (50 nM) and high (500 nM) Tag concentrations and in the presence or absence of ATP. Volume analyses of protein complexes bound to ssDNA regions are shown in the right panels of (A–C). Volumes consistent with monomeric Tag, smaller oligomers (dimers to hexamers), and higher order oligomers (double-hexamers) are indicated in the distributions. The volume distributions indicate predominantly monomeric Tag (∼100 nm^3) at 50 nM Tag (A), monomeric, dimeric, and trimeric intermediate complexes on the ssDNA at 500 nM Tag in the absence of ATP (B), and higher order oligomeric states (∼500 and ∼1200 nm^3) at 500 nM Tag and in the presence of ATP (C). (D) Volume analysis of 500 nM Tag in the absence of DNA shows predominantly monomeric protein also in the presence of ATP (∼40–100 nm^3).

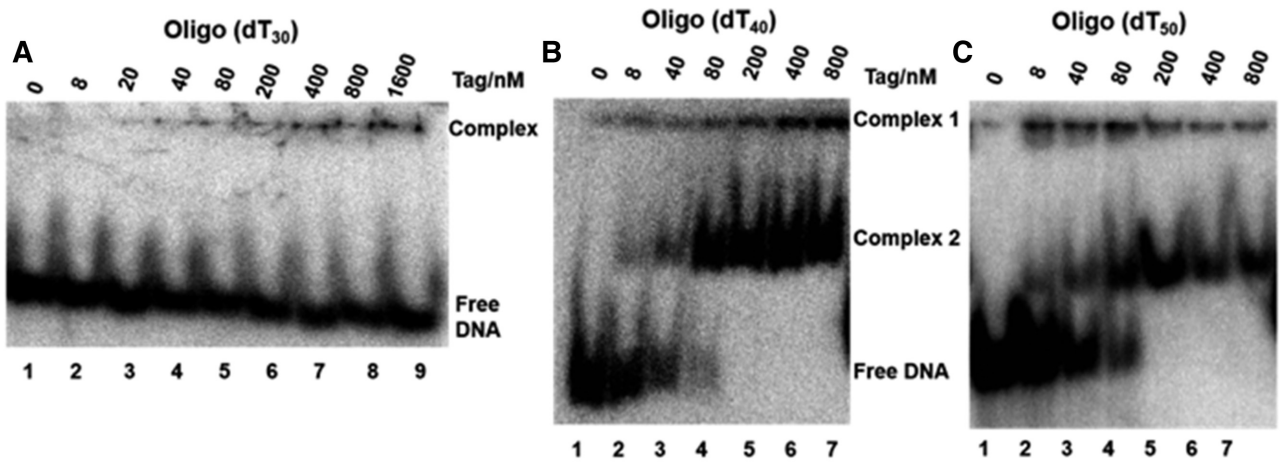

Figure 5. Length requirement for SV40 Tag binding to ssDNA. Increasing concentrations of SV40 Tag (concentrations as indicated, lanes 2 to 7 or 9) were incubated with 10 fmol of radioactively labeled oligo(dT)$_{30}$ (**A**), oligo(dT)$_{40}$ (**B**), or oligo(dT)$_{50}$ (**C**) and loaded on non-denaturing polyacrylamide gels (7%). For oligo(dT)$_{30}$, protein–DNA complexes were crosslinked with glutaraldehyde prior to gel electrophoresis. The protein-DNA complexes on oligo(dT)$_{40}$ and oligo(dT)$_{50}$ were loaded on the gels without prior crosslinking. In all experiments bound and free DNA was determined by autoradiography using a Fuji FLA5100 phosphorimager and Image Gauge analysis software. For comparison, lane 1 in each panel shows a DNA sample in the presence of only assay buffer.

Table 3. K_D values for Tag-poly(dT) and oligo(dT) ssDNA complex formation

	K_D (nM)
Poly(dT)*	40 ± 60
Oligo(dT20)**	n. d
Oligo(dT30)**	n. d.
Oligo(dT40)**	30±8
Oligo(dT50)**	10±7
Oligo(dT60)**	20±14
* value measured by DSF; ** values determined by EMSA	

oligo(dT)-ssDNA for efficient Tag binding is ∼40–50 nucleotides.

Coordinated ssDNA binding by RPA and Tag

Remarkably, the affinity we observed for Tag for the ∼50 nt oligonucleotides (10–20 nM) is in a similar range as that of replication protein A (RPA, the eukaryotic ssDNA-binding protein (61,84–86). RPA and Tag have further been shown to directly interact *via* the RPA70AB and RPA32C regions in RPA and the OBD domain in Tag (24,87–90). We investigated SV40 Tag and RPA interactions with 57 nt long ssDNA substrate using EMSA experiments (Figure 6A). The EMSA results for SV40 Tag by itself binding to ssDNA showed the existence of two different molecular weight complexes associated with ssDNA(GAPDH), Complex 1 and 2, likely representing hexameric (or double-hexameric) complexes and monomeric Tag bound to ssDNA, respectively (Figure 6A lanes 2–6 and Figure 1, panels C and D). When RPA was added, additional molecular weight complexes were observed. At low RPA and Tag concentrations (<2 nM of RPA, < 50 nM of Tag), Tag Complex 1 and 2 as well as monomeric RPA were bound independently to ssDNA (Figure 6A, lanes 8 and 14). Hereby, the formation of the RPA–ssDNA complex appears to reduce the amount of hexameric/double-hexameric Tag complexes binding to the ssDNA at least in part since the amount of low mobility Tag species (Complex 1) is decreased under these conditions whereas monomeric Tag–ssDNA complexes remain relatively unchanged. Increasing the RPA concentration (RPA > 3 nM and 40–80 nM Tag) strongly reduces the homo-hexameric (or double-hexameric) Tag-ssDNA species (Complex 1) but also the monomeric Tag protein in complex with ssDNA (Complex 2). Importantly, under these conditions a new species (Complex 3, black arrow in Figure 6A) with intermediate mobility between monomeric RPA and the homo-hexameric Tag Complex 1 can be seen that requires the presence of both Tag and RPA. For high RPA and Tag concentrations (≥6 and ≥400 nM, respectively), a second new complex species (Complex 4, gray arrow in Figure 6A) can further be detected, with lower mobility than Complex 3. To characterize and better understand these new complexes 3 and 4, we again applied AFM imaging.

For AFM analyses, we incubated Tag (500 nM) with RPA (10 nM) and the DNA substrate containing the 48 nt ssDNA region at ∼50% of the DNA length and analyzed the volumes of complexes bound at the ssDNA position (Figure 6B left and center; volume analyses of the individual proteins are shown in Supplemental Figure S7). The volume distributions show a broad peak centered at ∼1600 nm^3 consistent with the co-existence of multiple oligomeric species, and a major species at a volume of ∼200 nm^3 consistent with a heterodimeric complex (Figure 6B, middle). We confirmed the presence of RPA in these heterodimeric complexes by incubating the samples with an antibody that binds to RPA70, the largest subunit of the heterotrimeric RPA molecule, and that clearly shifted the volumes of protein-bound ssDNA complexes towards larger volumes (Figure 6B, right). The resulting volume distributions clearly showed a shift for both the dimeric and the oligomeric species towards larger volumes, indicat-

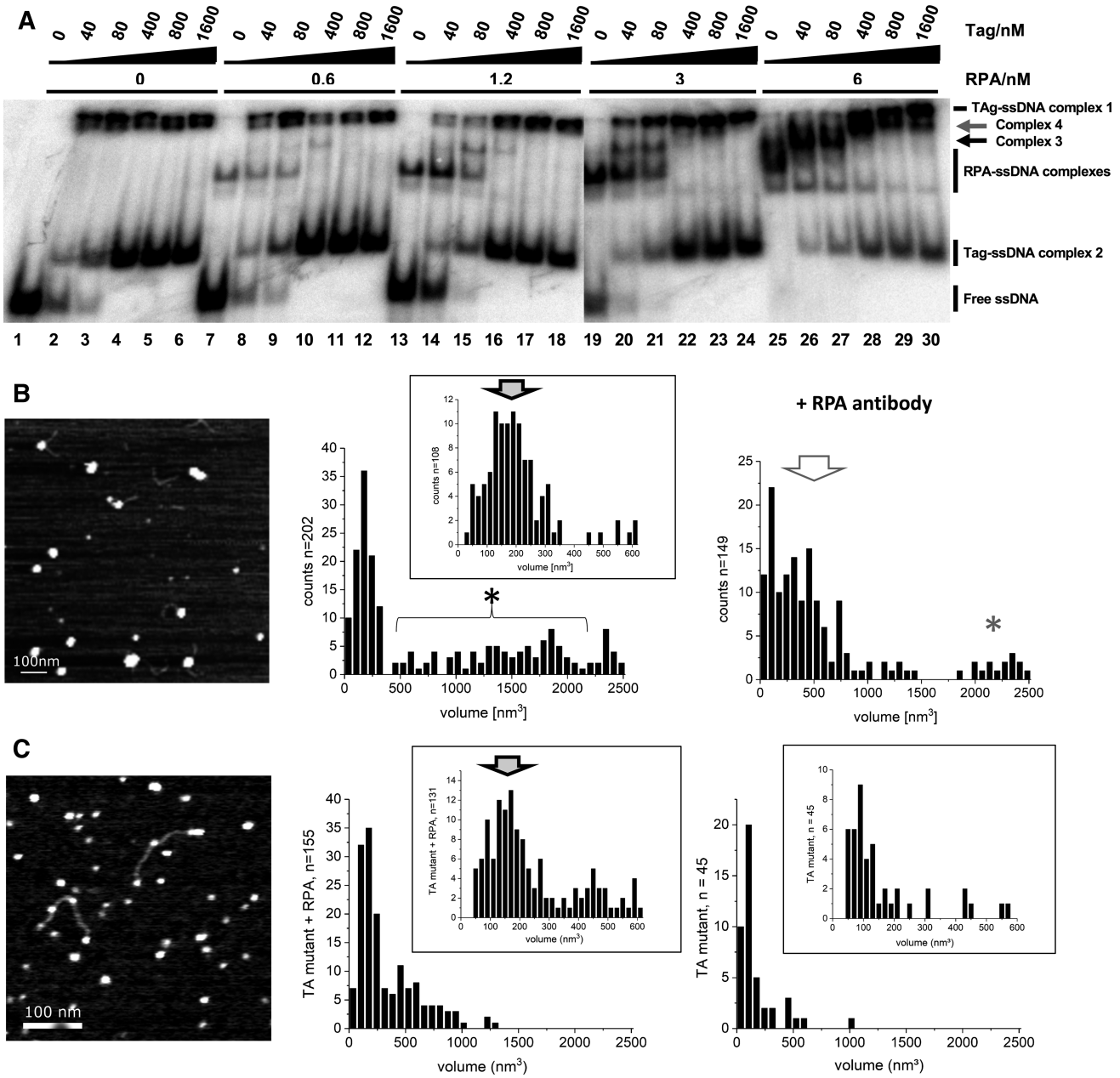

Figure 6. SV40 Tag and RPA interactions with ssDNA. (**A**) Increasing concentrations of SV40 Tag (40–1600 nM as indicated) were incubated with 10 fmol of GAPDH–ssDNA either in the absence (lanes 1–6) or in the presence of RPA at 0.6 nM (lanes 7–12), 1.2 nM (lanes 13–18), 3 nM (lanes 19–24), or 6 nM (lanes 25–30). The protein-DNA complexes were separated by non-denaturing PAGE (7% acrylamide) without crosslinking of the protein-DNA complexes. (**B**) AFM imaging of Tag and RPA incubated at 500 and 10 nM, respectively with DNA substrate containing a ssDNA region at ∼50% of the DNA length. Complexes were crosslinked with 0.1% glutaraldehyde prior to deposition for imaging. A representative AFM image (left) and volume analyses (center) indicate heterodimeric, RPA plus monomeric Tag (gray arrow in center inset), and large oligomeric complexes (marked with a black asterisk (*)) on the ssDNA. Samples were additionally incubated with an RPA antibody (right panel). The shifts in complex volumes in the presence of the RPA antibody confirm the presence of RPA in the (heterodimeric and -oligomeric) ssDNA bound complexes. The heterodimeric volumes (∼200 nm^3 in the absence of antibody, grey arrow in central panel inset) shift to 250–500 nm^3 in the presence of antibody (white arrow in right panel), revealing the presence of a heterodimeric RPA–Tag complex on ssDNA in the experiments. Consistently, control experiments with RPA alone showed volumes of ssDNA bound complexes that were approximately 100 nm^3 smaller than those for the mixed RPA-Tag samples, ∼100 nm^3 in the absence and ∼400 nm^3 in the presence of RPA antibody (Supplemental Figure S8). In addition, the presence of RPA in the oligomeric complexes (black asterisk (*) species from center plot) is supported by the shift of these intermediate volumes to higher volumes (2000–2500 nm^3 (gray asterisk (*) in right panel). The dominance of smaller oligomers after incubation with the antibody may hint at a partial disruption of large RPA-Tag complexes upon antibody binding. (**C**) AFM analyses of the monomeric $Tag_{131–627}$ (V350E/P417D) mutant incubated with RPA and the ssDNA containing DNA substrate. Volume analyses showed that $Tag_{131–627}$ (V350E/P417D) alone binds ssDNA exclusively in the monomeric form (right panel) whereas in the presence of RPA (center and a representative AFM image on the left) $Tag_{131–627}$ (V350E/P417D) forms predominantly heterodimers with RPA on the ssDNA (grey arrow in the inset of the central panel).

ing the presence of RPA in both complex types. The large shifts by ∼400 nm^3 with the antibody are slightly surprising and would suggest the binding of more than one antibody molecule to the complexes. The binding of more than one antibody to monomeric RPA, possibly as a dimeric antibody species, is, however, unlikely based on the distinct monomeric volume distribution observed for the antibody alone (Supplemental Figure S7C). A possible explanation for the larger volume shifts with the antibody is that the resulting complexes may contain large cavities and/or deviations from a globular shape, so that the envelope detected by the AFM topography scans would result in false high overall volumes. As a control, we incubated the ssDNA containing DNA substrate with RPA alone (10 nM, Supplemental Figure S8A) as well as with RPA followed by incubation with the RPA antibody (10 nM, Supplemental Figure S8B) as in the mixed Tag-RPA experiments. The measured volumes confirm monomeric RPA binding to the ssDNA under these conditions (∼100 nm^3 volume) and a shift by ∼400 nm^3 upon binding of RPA antibody to these monomeric RPA complexes. Based on these control experiments, we interpret the shift from ∼200 to ∼600 nm^3 in the mixed Tag-RPA samples as indication for a heterodimeric Tag-RPA complex bound to the ssDNA.

To verify that the heterodimeric Tag-RPA complex is indeed formed by monomeric Tag, we repeated the experiments using the previously described $Tag_{131–627}$ (V350E/P417D) variant (21). These mutations have been reported to efficiently disrupt oligomerisation of and ATP hydrolysis by Tag (21). Indeed, our AFM analyses of DNA bound $Tag_{131–627}$ (V350E/P417D) volumes clearly revealed exclusively monomeric Tag bound to ssDNA (Figure 6C right and Supplemental Figure S9A). $Tag_{131–627}$ (V350E/P417D) misses the N-terminal DnaJ domain and the C-terminal region after the helicase domain, resulting in a molecular weight reduction and yielding a ∼57 kDa protein compared to ∼82 kDa of full length Tag. The wild-type variant of this shortened construct (wild-type $Tag_{131–627}$) formed oligomeric complexes on the ssDNA, comparable to the full-length protein (Supplemental Figure S10). Consistent with previous reports (21), wild-type $Tag_{131–627}$ also displayed comparable ATPase activity as the full length protein in thin layer chromatography-based ATPase assays, while the V350E/P417D mutant showed a very reduced but detectable ATPase activity (data not shown). Further incubations of the monomeric Tag variant and RPA with ssDNA resulted in the predominant formation of protein-ssDNA complexes in AFM experiments with volumes consistent with a heterodimer containing Tag and RPA (Figure 6C, left and central panel). The measured volumes are consistent with the decrease in molecular weight of $Tag_{131–627}$ compared to the full-length protein. These data confirm the formation of RPA-Tag heterodimers by monomeric Tag.

Monomeric Tag is sufficient and necessary to stimulate DNA polymerase α-primase activity on ssDNA templates

AFM as well as EMSA data indicated stable complexes of monomeric Tag on ssDNA that can also form complexes with RPA. To investigate in more detail the functions of hexameric/double-hexameric and monomeric forms of Tag during viral DNA replication, we tested the ability of purified variants of Tag, wild-type $Tag_{131–627}$, which mainly binds ssDNA in its hexameric/double-hexameric form (Supplemental Figure S11A, right panel), and monomeric mutant $Tag_{131–627}$ (L286D/R567E), which associates with ssDNA exclusively as a high mobility complex (Supplemental Figure S11B), to stimulate DNA synthesis by Pol-prim. For this, we employed a model system for initiation and DNA synthesis on the lagging strand, using an unprimed natural ssDNA template in the absence and presence of RPA (35,36,57,91).

Full-length SV40 Tag has been reported to strongly stimulate Pol-prim activity on ssDNA (35,36,57,91). In our measurements, 0.6 μg of full length Tag, which binds to ssDNA as a monomer and a hexamer/double-hexamer (Figure 1 and Supplemental Figure S11A, left panel), stimulated primase plus DNA polymerase activity of Pol-prim on ssDNA nearly 8-fold (∼800%, Supplemental Figure S12, compare second with first column). Interestingly, monomeric $Tag_{131–627}$ (L286D/R567E) efficiently stimulated DNA synthesis on ssDNA by Pol-prim (Figure 7A) with maximum enhancement of ∼5.5-fold (∼550%) for 1 μg of protein. In contrast to the monomeric variant and to full length Tag, wild type $Tag_{131–627}$ inhibited Pol-prim activity on ssDNA in a concentration-dependent manner (Figure 7B). Adding 1 μg of $Tag_{131–627}$ decreased the Pol-prim activity to ∼30%.

In the presence of RPA (0.5 μg), Pol-prim enzyme activity including binding to ssDNA, primase function and subsequent DNA synthesis (dNMP incorporation) are strongly inhibited. In experiments performed in parallel, the addition of RPA but omission of Tag resulted in only 16% Pol-prim activity compared to 100% in the absence of RPA (see Supplemental Figure S12, third column, and dashed and continuous curve at 0 μg Tag in Figure 7A). Primase and DNA synthesis activity of Pol-prim were strongly stimulated by addition of full length Tag to the RPA-ssDNA template. Maximum stimulation of Pol-prim by 29-fold compared to RPA–ssDNA was observed at 0.6 μg of full length Tag (Supplemental Figure S12, fourth and third column). This corresponds to a maximum relative Pol-prim synthesis rate of ∼450% on the RPA–ssDNA template compared to ∼800% in the absence of RPA. Notably, adding monomeric $Tag_{131–627}$ (L286D/R567E) protein to the RPA-coated ssDNA clearly led to efficient synthesis of primers and DNA by Pol-prim (up to 25-fold stimulation, Figure 7A), similar as for the hexamer and monomer-forming full-length protein. The relative synthesis rate increased to ∼400% (compared to 550% in the absence of RPA, Figure 7A dashed line, and compared to ∼450% maximum stimulation by full length Tag on RPA-ssDNA, Supplemental Figure S12, last column). Interestingly the addition of wild type $Tag_{131–627}$ and RPA synergistically reduced Pol-prim activity on ssDNA (Figure 7B, columns 5 and 6). These data strongly suggest that the hexameric/double-hexameric complexes formed by SV40 $Tag_{131–627}$ on ssDNA are not able to stimulate the Pol-prim activity on ssDNA whereas the monomeric Tag protein binds to ssDNA in the presence of RPA and efficiently stimulates Pol-prim-dependent DNA synthesis, thus initiating DNA replication. Our conclusions

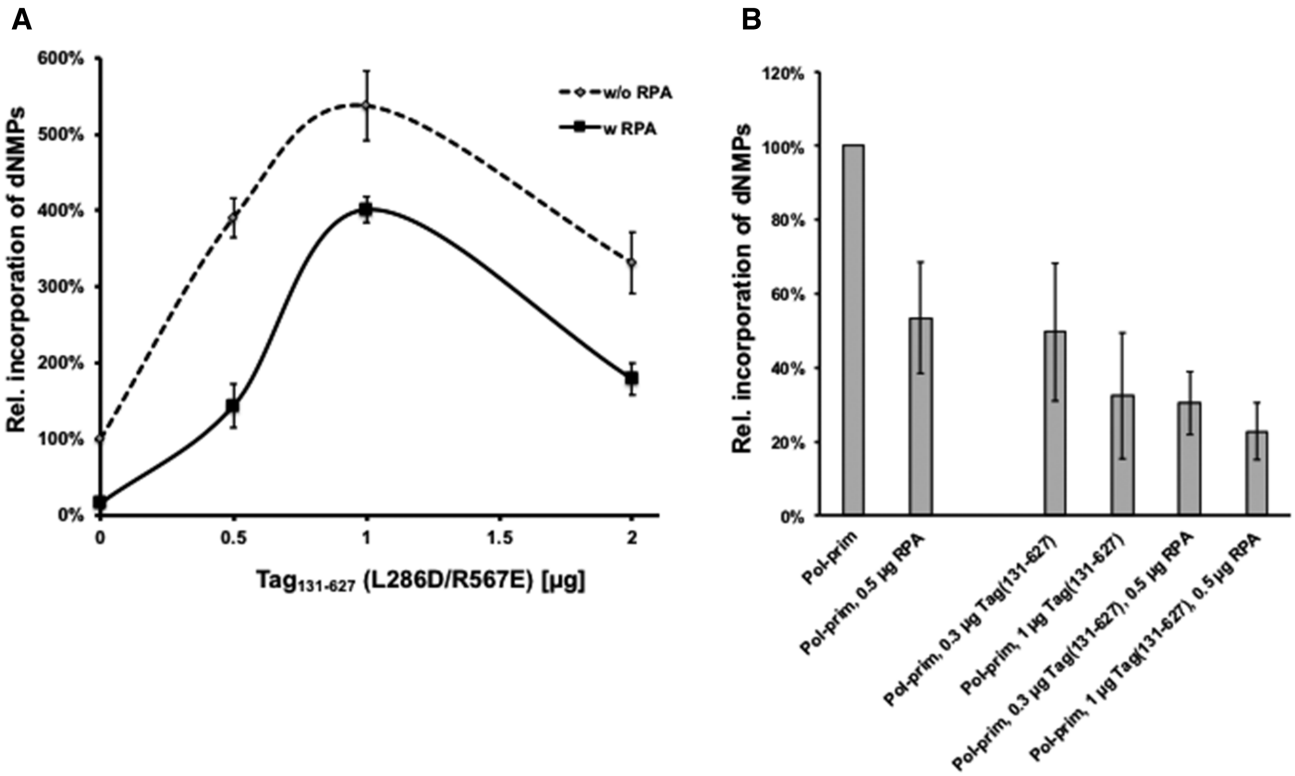

Figure 7. Modulation of Pol-prim-dependent DNA synthesis on ssDNA by SV40 large T antigen variant proteins. The two replication proteins, RPA and viral Tag, physically and functionally interact with Pol-prim during the initiation and elongation step of DNA synthesis on ssDNA templates (8). (**A**) The relative incorporation of dNMPs by Pol-prim in a primase-initiated DNA synthesis assay on unprimed ssDNA was measured in the absence and presence of human RPA (dashed and solid line, respectively) using increasing amounts of a monomeric SV40 Tag variant. Pol-prim stimulation by the monomeric Tag variant is only slightly weaker than by full length wild-type Tag (less than a factor of 2, Supplemental Figure S12). **(B)** The relative incorporation of dNMPs by Pol-prim on unprimed ssDNA was determined in the absence and presence of human RPA (first and second column, respectively). Addition of $Tag_{131–627}$ to the assay in absence of RPA inhibited the reaction in a concentration-dependent manner (third and fourth column). Adding $Tag_{131–627}$ to assays containing 0.5 μg of RPA increased the extend of the inhibition (compare column 2 with the two last columns on the right). In all assays (panels A and B) the background radioactivity determined in a parallel assay performed in the absence of Pol-prim (negative control) was subtracted from each value before calculation of the incorporation data. The averages of the DNA synthesis from three independent experiments and their standard deviations are presented. In both panels the DNA synthesis of Pol-prim on unprimed ssDNA alone was arbitrarily set as 100% in each assay. Pol-prim activities measured (in the absence of Tag) on both templates (ssDNA and RPA-ssDNA) in our assays are consistent with previously published data (57).

are summarized in the model shown in Figure 8 and will be discussed in the following section.

DISCUSSION

At the start of viral DNA replication, double-hexameric SV40 Tag binds to and destabilises origin DNA, and two SV40 Tag helicase hexamers then move bi-directionally on the leading strands of a replication bubble in 3′ to 5′ direction (8). This helicase activity produces stretches of ssDNA (Figure 8A) which are rapidly coated and protected by RPA. Tag hexamers themselves have also been proposed to assist in the loading of RPA onto the evolving ssDNA (8,24). Next SV40 Tag allows the initiation of DNA replication in the origin on the leading strand by Pol-prim. After producing an RNA-DNA primer, the latter is transferred to Pol δ which then processively translocates along the ssDNA in 3′ to 5′ direction with the help of PCNA and synthesises leading strand DNA (8,16) (see also model in Figure 8B). On the lagging strand the situation is more complicated: RPA is expected to bind to the ssDNA produced by the helicase activity of SV40 Tag hexamer. However, ssDNA associated with RPA is a very inefficient substrate for primase (see e.g. Figure 7B). Although Pol-prim primase synthesises primers on ssDNA without additional helper function the enzyme is effectively inactive on RPA-coated ssDNA substrates (35,36,57). Intriguingly, our results suggest that interactions of monomeric Tag with ssDNA cooperate with RPA during the initiation of Okazaki fragment synthesis on the lagging strand, as will be discussed below.

Although SV40 Tag interactions with ssDNA substrates have been previously reported (48,49,51,52), the affinities and the length requirement of these ssDNA interactions for full length Tag have not been investigated in detail, despite their crucial importance during DNA replication initiation. A detailed knowledge of the properties of Tag binding to ssDNA is required to better delineate the complex mechanism of coordination of various cellular proteins binding simultaneously or consecutively to DNA to initiate replication (46,49,51,52,55). Our studies show that full-length SV40 Tag binds to ssDNA with high affinity irrespective of sequence and base composition. Full length Tag bound with significantly lower affinity to non-specific dsDNA (apparent $K_D > 1$ μM) than ssDNA (apparent K_D values are ∼100

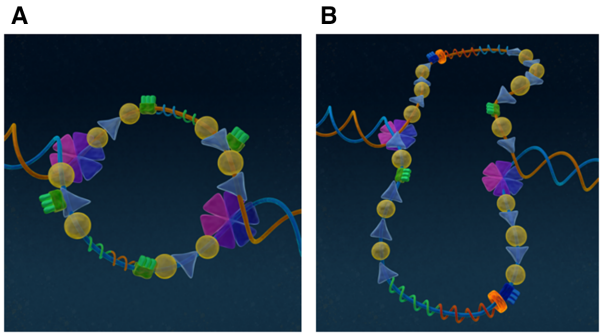

Figure 8. Model of RPA loading on ssDNA by SV40 Tag in replication initiation. RPA and Tag perform numerous protein-protein and protein-DNA interactions on ssDNA templates during viral DNA replication. Our data show high affinity binding and high specificity for ssDNA over ds-DNA binding of monomeric (blue triangles) as well as hexameric Tag (six blue-pink triangles). In our model, RPA (yellow discs) and monomeric Tag both support hexameric Tag helicase activity by filling up the evolving ss-DNA in its wake. In addition, monomeric Tag is also involved in loading of the priming polymerase in lagging strand synthesis. (**A**) Early stage of SV40 DNA replication with hexameric Tag helicase on the leading strand unwinding the two replication forks. The primase of Pol-prim (green symbols) produces the RNA-DNA primer on the leading strand (RNA shown in green, DNA in brown/blue). (**B**) Pol δ (blue symbol) associated with a PCNA ring (redorange-colored ring symbol) takes over leading strand DNA synthesis from Pol-prim. On the lagging strand, Pol-prim is loaded by monomeric Tag to initiate Okazaki fragment synthesis. For simplification Topoisomerase I and Replications Factor C are omitted in the model.

nM in our EMSA and ∼30 nM in DSF experiments), which is consistent with estimations determining K_i values using full length and Tag deletion mutants (46,48). Consistently, AFM positional analyses revealed that a 48 nucleotide-long ssDNA stretch was bound by Tag with high preference (> ∼1000-fold) over the surrounding dsDNA regions. Interestingly, the ssDNA binding affinity of Tag was even higher than or comparable to that to its origin target site in ds-DNA in EMSA and DSF (Tables 1 and 2). However, SV40 Tag binding to ssDNA depended strongly on the length of the ssDNA substrate. The protein bound ssDNAs with lengths >40 nucleotides with high affinity (K_D ∼10 nM, Table 3). In contrast, ssDNA sequences with less than 40 nucleotides displayed very weak binding (see Figure 5 and Table 3). These ssDNA binding requirements and affinities of the SV40 Tag helicase are similar to those of Mcm2–7, the eukaryotic replicative helicase machinery, which requires an oligo(dT) length of longer than 40 nucleotides for optimal binding with affinities of K_D = 38 nM (92). Moreover, the apparent K_D of SV40 Tag binding to ssDNA of ∼10 nM (for ssDNA lengths of >40 nucleotides; Table 3) is comparable to that of human RPA, which has been reported to bind to 34 nt long ssDNA of mixed sequence with a K_D of ∼38 nM in surface plasmon resonance measurements (61). However, the affinity of RPA to ssDNA depends on the DNA length and sequence (85) and we measured a K_D for our ssDNA substrate (ssDNA(GAPDH), 57 nt) and a K_D value of ∼10 nM using EMSA (data not shown), close to the affinity of Tag to the same ssDNA sequence.

Our experiments further showed that SV40 Tag forms at least two stable complexes with ssDNA. Low and high mobility SV40 Tag–ssDNA complexes in our EMSA studies correspond most likely to SV40 Tag hexamers or double-hexamer, which are known to assemble on the origin of replication (7,17–19), and monomers, respectively. In contrast, our EMSA data showed exclusively SV40 Tag hexamers or double-hexamers but no monomers bound to ds-DNA. Furthermore, monomeric and oligomeric Tag complexes formed independently of each other on ssDNA in our experiments, as revealed by crosslinking. The predominance of monomeric and hexameric Tag complexes on ssDNA was also supported by our AUC analyses. Furthermore, single molecule imaging by AFM allowed us to characterise the individual, crosslinked complexes with ss-DNA, showing monomeric and double-hexameric species in the presence of ATP in a concentration-dependent manner. Efficient Tag oligomerisation on ssDNA was dependent on the presence of ATP in AFM, AUC and native PAGE experiments. Previous studies suggested that ATP binding supports Tag assembly with the origin of replication as hexamer and double-hexamer (18,82,83,93,94) and that ATP hydrolysis by Tag is then required for destabilisation and denaturation of the SV40 origin to provide access to other replication factors for coordinated replication initiation (95). Furthermore, stimulation of Tag AT-Pase activity by ssDNA has also previously been reported (96). We show here, using AUC, AFM, and native PAGE, that ATP and ssDNA individually stimulate SV40 Tag oligomerisation to similar degrees and that this stimulation is significantly enhanced in the presence of both ATP and ssDNA. Our results are consistent with a model, in which Tag binding to ssDNA in turn enhances ATP binding, leading to augmented hexamer/double-hexamer formation and ATPase activity. Importantly, similar populations of monomeric and hexameric/double-hexameric Tag were observed on ssDNA in EMSA, AUC, and AFM. Monomers through hexamers of SV40 Tag have been reported to interact with dsDNA containing region I and II of SV40 origin of replication in the process of stepwise assembly of hexameric/double-hexameric SV40 Tag complexes (44). It has been hypothesized that Tag monomers would bind to dsDNA and provide the nuclei for the formation of hexamers and double-hexamers without a specific function of their own (17,18). In contrast, our findings indicate that the monomeric form of SV40 Tag binds to ss-DNA with high affinity in a sequence-independent manner and that apparent K_D values of monomeric Tag are in the same range as those of the hexameric or double-hexameric forms for ssDNA, suggesting a potential independent role of monomeric Tag in DNA replication.

The loading of RPA onto ssDNA by Tag and the recruitment of the priming enzyme complex, Pol-prim, by the RPA-Tag complex is believed to play an integral role in replication initiation (6,22–25). Our EMSA and AFM analyses demonstrate the formation of heterodimeric Tag-RPA complexes on ssDNA (involving monomeric Tag), as well as hexameric or double-hexameric Tag complexes associated with RPA. The ability of monomeric Tag to independently form a heterodimeric complex with RPA on ssDNA is further strongly supported by our AFM experiments using the SV40 $Tag_{131–627}$ (V350E/P417D) variant of the protein, in which the interface for Tag oligomerisation is disrupted (21). Moreover, using the SV40 $Tag_{131–627}$ (L286D/R567E)

protein variant that – similar to V350E/P417D – exclusively forms monomers (21), we showed that Pol-prim activity is stimulated strongly by monomeric Tag on ssDNA templates in the absence and presence of RPA. In fact, the degree of enhancement of DNA synthesis by Pol-prim was similar for the monomeric variant and for full length Tag (which is capable of forming higher order oligomers as well as monomers). The activity of $Tag_{131–627}$ (L286D/R567E) in these assays indicates for the first time that all functional and physical interactions of SV40 Tag with ssDNA, RPA and Pol-prim to initiate Okazaki fragment synthesis reside in the SV40 Tag core residues, aa131 to aa627. However, wild type $Tag_{131–627}$, which bound to ssDNA exclusively as high molecular weight complexes with slow mobility (hexamers/double-hexamers) in our EMSA studies, did not stimulate Pol-prim on ssDNA templates but inhibited the activity of Pol-prim on these templates. Our data thus show that monomeric but not hexameric forms of SV40 Tag as previously suggested (35,36,91), stimulate the initiation and elongation of DNA synthesis by Pol-prim on RPA-bound ssDNA, which is a model system for lagging strand synthesis (Figures 7 and summarised in the model of Figure 8).

Our findings led us to suggest a new model for the role of SV40 Tag in leading and lagging strand synthesis (Figure 8). We speculate that the low affinity of Pol-prim (in the high micromolar range, data not shown) prevents its binding to ssDNA in the presence of high affinity RPA–ssDNA complexes. Physical interactions of RPA with or competitive ssDNA binding by SV40 Tag monomers may favour recruitment of Pol-prim by monomeric Tag-RPA-ssDNA or Tag-ssDNA complexes to initiate DNA synthesis on these templates. This model is compatible with previous reports that interactions of the Tag origin-binding domain (OBD) with the C-terminal domain of RPA subunit RPA32 are required for the initiation of lagging strand DNA synthesis (35). Our new model is also consistent with previous findings that SV40 Tag helicase activity, a function of hexameric Tag, is not required for initiation of Okazaki fragment by Pol-prim (91). A similar problem also arises in other DNA metabolic pathways such as homologous recombination where the initial RPA–ssDNA complexes are replaced by Rad51 filaments to allow for strand invasion to occur (97,98). Interestingly, similar as proposed here for Tag monomers, monomeric replication mediator protein Rad52 has been shown to interact with RPA (DBD-D on RPA32) and thus destabilize RPA–ssDNA complexes formed during the initial steps of homologous recombination (99).

Our data strongly suggest a functional role for monomeric SV40 Tag on its own independent of the oligomeric complexes in SV40 DNA replication. Tag monomers may function as auxiliary factors for primase recruitment to initiate Okazaki fragments on the lagging strand (see Figure 8B). Our model of DNA replication initiation by SV40 Tag (Figure 8) also offers new insight also for cellular chromosomal DNA replication. SV40 Tag as a hexameric helicase progresses in 3′ to 5′ direction and is thus associated with leading strand DNA synthesis at the replication fork similar to the eukaryotic CMG helicase (1,2,8,17). Our data suggest that differently to previously published models the hexameric Tag helicase at the replication fork does not simultaneously provide the auxilliary activity for the initiation of Okazaki fragments on the lagging strand (Figure 8B; (8,91)). This would also explain current discrepancies in *in vitro* replication assays, where concentrations required for Tag are typically similar or slightly higher than those of RPA (∼200 nM versus ∼150 nM), with topoisomerase I and Pol-prim present at much lower concentrations (∼8 and ∼5 nM, respectively). Similarly, in currently established cellular DNA replication systems, the factors on leading strand DNA synthesis are sufficient for equal incorporation rates *in vitro* as *in vivo*, but show very low DNA synthesis activity on the lagging strand (53), suggesting that auxiliary factors for the primase are still lacking or not fully defined in the *in vitro* systems. Consistent with previously published views (reviewed in 8), our model suggests that two hexamers of SV40 Tag unwind the origin dsDNA to initiate DNA replication (blue-pink triangles assembled to a hexameric helicase in Figure 8). In contrast to established opinion that hexameric SV40 Tag at the replication fork would assist Okazaki fragment initiation (8), our model presented here proposes independent monomeric SV40 Tag molecules (blue triangles in Figure 8) that support Okazaki fragment synthesis by Pol-prim (green symbols) in the presence of RPA (yellow discs). Finally, binding sites in RPA for Cdc45 and Tag are highly similar and are located in DBD-A, B and F of the RPA70 subunit as well as the C-terminal region of RPA32 (24,61,100). Interestingly, RPA has been shown to interact with both Cdc45 in eukaryotic and Tag in viral replication initiation similarly, and independent of their ssDNA binding function (24,61,79,88). Thus, our model for the unloading of RPA and the initiation of Okazaki fragment synthesis has important implications for our understanding of cellular DNA replication and provides additional insights into a holistic mechanism of replication initiation.

SUPPLEMENTARY DATA

Supplementary Data are available at NAR Online.

ACKNOWLEDGEMENTS

The authors thank Ms Patricia Nyland for expert technical assistance, Dr Anna Szambowska, Jena, for providing RPA and RPA antibody, and Dr Zoë Popper, NUI Galway, for providing a TLC chamber. The authors also thank Drs. Lars Schönemann and Maren Bleckmann of the Recombinant Protein Expression Facility (University of Würzburg) for their expert purification of wild type and mutant $Tag_{131–627}$, and Maciej Doczyk (NUI Galway) for his graphical work.

FUNDING

Else Kröner-Fresenius-Stiftung (EKFS) [2013_A215]; PML Consortium (Washington, USA) [RIB1099] to H.P.N. Funding for open access charge: Funding by NUI Galway and University of Würzburg.
Conflict of interest statement. None declared.

REFERENCES

1. Bleichert,F., Botchan,M.R. and Berger,J.M. (2017) Mechanisms for initiating cellular DNA replication. *Science*, **355**, eaah6317.
2. Burgers,P.M.J. and Kunkel,T.A. (2017) Eukaryotic DNA replication fork. *Annu. Rev. Biochem.*, **86**, 417–438.
3. O'Donnell,M., Langston,L. and Stillman,B. (2013) Principles and concepts of DNA replication in bacteria, archaea, and eukarya. *Cold Spring Harb. Perspect. Biol.*, **5**, a010108.
4. Zhang,D. and O'Donnell,M. (2016) The eukaryotic replication machine. *The Enzymes*, **39**, 191–229.
5. Deegan,T.D. and Diffley,J.F. (2016) MCM: one ring to rule them all. *Curr. Opin. Struct. Biol.*, **37**, 145–151.
6. An,P., Saenz Robles,M.T. and Pipas,J.M. (2012) Large T antigens of polyomaviruses: amazing molecular machines. *Ann. Rev. Microbiol.*, **66**, 213–236.
7. Fanning,E. and Zhao,K. (2009) SV40 DNA replication: from the A gene to a nanomachine. *Virology*, **384**, 352–359.
8. Sowd,G.A. and Fanning,E. (2012) A wolf in sheep's clothing: SV40 co-opts host genome maintenance proteins to replicate viral DNA. *PLoS Pathog.*, **8**, e1002994.
9. Waga,S., Bauer,G. and Stillman,B. (1994) Reconstitution of complete SV40 DNA replication with purified replication factors. *J. Biol. Chem.*, **269**, 10923–10934.
10. Fanning,E. and Knippers,R. (1992) Structure and function of simian virus 40 large tumor antigen. *Annu. Rev. Biochem.*, **61**, 55–85.
11. Fanning,E., Zhao,X. and Jiang,X. (2009) Polyomavirus Life Cycle. In: Damania,B and Pipas,JM (eds). *DNA Tumor Viruses*. Springer Science + Business Media, NY, pp. 1–24.
12. Bullock,P.A., Seo,Y.S. and Hurwitz,J. (1991) Initiation of simian virus 40 DNA synthesis *in vitro*. *Mol. Cell Biol.*, **11**, 2350–2361.
13. Li,J.J. and Kelly,T.J. (1984) Simian virus 40 DNA replication in vitro. *Proc. Natl. Acad. Sci. U.S.A.*, **81**, 6973–6977.
14. Stillman,B. (2008) DNA polymerases at the replication fork in eukaryotes. *Mol. Cell*, **30**, 259–260.
15. Stillman,B. (2015) Reconsidering DNA polymerases at the replication fork in eukaryotes. *Mol. Cell*, **59**, 139–141.
16. Waga,S. and Stillman,B. (1998) The DNA replication fork in eukaryotic cells. *Annu. Rev. Biochem.*, **67**, 721–751.
17. Borowiec,J.A., Dean,F.B., Bullock,P.A. and Hurwitz,J. (1990) Binding and unwinding–how T antigen engages the SV40 origin of DNA replication. *Cell*, **60**, 181–184.
18. Borowiec,J.A. and Hurwitz,J. (1988) ATP stimulates the binding of simian virus 40 (SV40) large tumor antigen to the SV40 origin of replication. *Proc. Natl. Acad. Sci. U.S.A.*, **85**, 64–68.
19. Li,D., Zhao,R., Lilyestrom,W., Gai,D., Zhang,R., DeCaprio,J.A., Fanning,E., Jochimiak,A., Szakonyi,G. and Chen,X.S. (2003) Structure of the replicative helicase of the oncoprotein SV40 large tumour antigen. *Nature*, **423**, 512–518.
20. Wessel,R., Schweizer,J. and Stahl,H. (1992) Simian virus 40 T-antigen DNA helicase is a hexamer which forms a binary complex during bidirectional unwinding from the viral origin of DNA replication. *J. Virol.*, **66**, 804–815.
21. Chang,Y.P., Xu,M., Machado,A.C., Yu,X.J., Rohs,R. and Chen,X.S. (2013) Mechanism of origin DNA recognition and assembly of an initiator-helicase complex by SV40 large tumor antigen. *Cell Rep.*, **3**, 1117–1127.
22. Chen,J., Le,S., Basu,A., Chazin,W.J. and Yan,J. (2015) Mechanochemical regulations of RPA's binding to ssDNA. *Sci. Rep.*, **5**, 9296.
23. Chen,R. and Wold,M.S. (2014) Replication protein A: single-stranded DNA's first responder: dynamic DNA-interactions allow replication protein A to direct single-strand DNA intermediates into different pathways for synthesis or repair. *Bioessays*, **36**, 1156–1161.
24. Jiang,X., Klimovich,V., Arunkumar,A.I., Hysinger,E.B., Wang,Y., Ott,R.D., Guler,G.D., Weiner,B., Chazin,W.J. and Fanning,E. (2006) Structural mechanism of RPA loading on DNA during activation of a simple pre-replication complex. *EMBO J.*, **25**, 5516–5526.
25. Wold,M.S. (1997) Replication protein A: a heterotrimeric, single-stranded DNA-binding protein required for eukaryotic DNA metabolism. *Annu. Rev. Biochem.*, **66**, 61–92.
26. Simmons,D.T., Trowbridge,P.W. and Roy,R. (1998) Topoisomerase I stimulates SV40 T antigen-mediated DNA replication and inhibits T antigen's ability to unwind DNA at nonorigin sites. *Virology*, **242**, 435–443.
27. Fanning,E., Klimovich,V. and Nager,A.R. (2006) A dynamic model for replication protein A (RPA) function in DNA processing pathways. *Nucleic Acids Res.*, **34**, 4126–4137.
28. Nasheuer,H.P., Pospiech,H. and Syväoja,J. (2007) In: Lankenau,DH (ed). *Genome Integrity: Facets and Perspectives*. Springer, Genome Dynamics & Stability, NY, Vol. **1**, pp. 27–68.
29. Stadlbauer,F., Voitenleitner,C., Brückner,A., Fanning,E. and Nasheuer,H.P. (1996) Species-specific replication of simian virus 40 DNA in vitro requires the p180 subunit of human DNA polymerase α-primase. *Mol. Cell Biol.*, **16**, 94–104.
30. Fortune,J.M., Stith,C.M., Kissling,G.E., Burgers,P.M. and Kunkel,T.A. (2006) RPA and PCNA suppress formation of large deletion errors by yeast DNA polymerase delta. *Nucleic Acids Res.*, **34**, 4335–4341.
31. Maga,G., Stucki,M., Spadari,S. and Hübscher,U. (2000) DNA polymerase switching: I. Replication factor C displaces DNA polymerase alpha prior to PCNA loading. *J. Mol. Biol.*, **295**, 791–801.
32. Mossi,R., Keller,R.C., Ferrari,E. and Hübscher,U. (2000) DNA polymerase switching: II. Replication factor C abrogates primer synthesis by DNA polymerase alpha at a critical length. *J. Mol. Biol.*, **295**, 803–814.
33. Nethanel,T. and Kaufmann,G. (1990) Two DNA polymerases may be required for synthesis of the lagging DNA strand of simian virus 40. *J. Virol.*, **64**, 5912–5918.
34. Yuzhakov,A., Kelman,Z., Hurwitz,J. and O'Donnell,M. (1999) Multiple competition reactions for RPA order the assembly of the DNA polymerase delta holoenzyme. *EMBO J.*, **18**, 6189–6199.
35. Arunkumar,A.I., Klimovich,V., Jiang,X., Ott,R.D., Mizoue,L., Fanning,E. and Chazin,W.J. (2005) Insights into hRPA32 C-terminal domain-mediated assembly of the simian virus 40 replisome. *Nat. Struct. Biol.*, **12**, 332–339.
36. Weisshart,K., Förster,H., Kremmer,E., Schlott,B., Grosse,F. and Nasheuer,H.P. (2000) Protein-protein interactions of the primase subunits p58 and p48 with simian virus 40 T antigen are required for efficient primer synthesis in a cell-free system. *J. Biol. Chem.*, **275**, 17328–17337.
37. Vaithiyalingam,S., Warren,E.M., Eichman,B.F. and Chazin,W.J. (2010) Insights into eukaryotic DNA priming from the structure and functional interactions of the 4Fe-4S cluster domain of human DNA primase. *Proc. Natl. Acad. Sci. U.S.A.*, **107**, 13684–13689.
38. Baranovskiy,A.G., Babayeva,N.D., Zhang,Y., Gu,J., Suwa,Y., Pavlov,Y.I. and Tahirov,T.H. (2016) Mechanism of concerted RNA-DNA primer synthesis by the human primosome. *The J. Biol. Chem.*, **291**, 10006–10020.
39. Baranovskiy,A.G. and Tahirov,T.H. (2017) Elaborated action of the human primosome. *Genes*, **8**, 62.
40. Hübscher,U., Maga,G. and Spadari,S. (2002) Eukaryotic DNA polymerases. *Annu. Rev. Biochem.*, **71**, 133–163.
41. Hübscher,U., Nasheuer,H.P. and Syväoja,J. (2000) Eukaryotic DNA polymerases, a growing family. *Trends Biochem. Sci.*, **25**, 143–147.
42. Bochkareva,E., Martynowski,D., Seitova,A. and Bochkarev,A. (2006) Structure of the origin-binding domain of simian virus 40 large T antigen bound to DNA. *EMBO J.*, **25**, 5961–5969.
43. Lorimer,H.E., Wang,E.H. and Prives,C. (1991) The DNA-binding properties of polyomavirus large T antigen are altered by ATP and other nucleotides. *J. Virol.*, **65**, 687–699.
44. Mastrangelo,I.A., Hough,P.V.C., Wall,J.S., Dodson,M., Dean,F.B. and Hurwitz,J. (1989) ATP-dependent assembly of double hexamers of SV40 T antigen at the viral origin of DNA replication. *Nature*, **338**, 658–662.
45. Meinke,G., Phelan,P., Moine,S., Bochkareva,E., Bochkarev,A., Bullock,P.A. and Bohm,A. (2007) The crystal structure of the SV40 T-antigen origin binding domain in complex with DNA. *PLoS Biol.*, **5**, e23.
46. Runzler,R., Thompson,S. and Fanning,E. (1987) Oligomerization and origin DNA-binding activity of simian virus 40 large T antigen. *J. Virol.*, **61**, 2076–2083.
47. Uhlmann-Schiffler,H., Seinsoth,S. and Stahl,H. (2002) Preformed hexamers of SV40 T antigen are active in RNA and origin-DNA unwinding. *Nucleic Acids Res.*, **30**, 3192–3201.

48. Fradet-Turcotte,A., Vincent,C., Joubert,S., Bullock,P.A. and Archambault,J. (2007) Quantitative analysis of the binding of simian virus 40 large T antigen to DNA. *J. Virol.*, **81**, 9162–9174.
49. Meinke,G., Phelan,P.J., Fradet-Turcotte,A., Bohm,A., Archambault,J. and Bullock,P.A. (2011) Structure-based analysis of the interaction between the simian virus 40 T-antigen origin binding domain and single-stranded DNA. *J. Virol.*, **85**, 818–827.
50. Reese,D.K., Meinke,G., Kumar,A., Moine,S., Chen,K., Sudmeier,J.L., Bachovchin,W., Bohm,A. and Bullock,P.A. (2006) Analyses of the interaction between the origin binding domain from simian virus 40 T antigen and single-stranded DNA provide insights into DNA unwinding and initiation of DNA replication. *J. Virol.*, **80**, 12248–12259.
51. Wu,C., Edgil,D. and Simmons,D.T. (1998) The origin DNA-binding and single-stranded DNA-binding domains of simian virus 40 large T antigen are distinct. *J. Virol.*, **72**, 10256–10259.
52. Wu,C., Roy,R. and Simmons,D.T. (2001) Role of single-stranded DNA binding activity of T antigen in simian virus 40 DNA replication. *J. Virol.*, **75**, 2839–2847.
53. Yeeles,J.T.P., Janska,A., Early,A. and Diffley,J.F.X. (2017) How the eukaryotic replisome achieves rapid and efficient DNA replication. *Mol. Cell*, **65**, 105–116.
54. Kurat,C.F., Yeeles,J.T.P., Patel,H., Early,A. and Diffley,J.F.X. (2017) Chromatin controls DNA replication origin selection, lagging-strand synthesis, and replication fork rates. *Mol. Cell*, **65**, 117–130.
55. Foster,E.C. and Simmons,D.T. (2010) The SV40 large T-antigen origin binding domain directly participates in DNA unwinding. *Biochemistry*, **49**, 2087–2096.
56. Collins,K.L. and Kelly,T.J. (1991) The effects of T antigen and replication protein A on the initiation of DNA synthesis by DNA polymerase a-primase. *Mol. Cell Biol.*, **11**, 2108–2115.
57. Melendy,T. and Stillman,B. (1993) An interaction between replication protein A and SV40 T antigen appears essential for primosome assembly during SV40 DNA replication. *J. Biol. Chem.*, **268**, 3389–3395.
58. Brückner,A., Stadlbauer,F., Guarino,L.A., Brunahl,A., Schneider,C., Rehfuess,C., Prives,C., Fanning,E. and Nasheuer,H.P. (1995) The mouse DNA polymerase a-primase subunit p48 mediates species- specific replication of polyomavirus DNA in vitro. *Mol. Cell Biol.*, **15**, 1716–1724.
59. Tikhanovich,I., Liang,B., Seoighe,C., Folk,W.R. and Nasheuer,H.P. (2011) Inhibition of human BK polyomavirus replication by small noncoding RNAs. *J. Virol.*, **85**, 6930–6940.
60. Henricksen,L.A., Umbricht,C.B. and Wold,M.S. (1994) Recombinant replication protein A: expression, complex formation, and functional characterization. *J. Biol. Chem.*, **269**, 11121–11132.
61. Szambowska,A., Tessmer,I., Prus,P., Schlott,B., Pospiech,H. and Grosse,F. (2017) Cdc45-induced loading of human RPA onto single-stranded DNA. *Nucleic Acids Res.*, **45**, 3217–3230.
62. Weisshart,K., Pestryakov,P., Smith,R.W., Hartmann,H., Kremmer,E., Lavrik,O. and Nasheuer,H.P. (2004) Coordinated regulation of replication protein A activities by its subunits p14 and p32. *J. Biol. Chem.*, **279**, 35368–35376.
63. Sambrook,J., Fritsch,E.F. and Maniatis,T. (1989) In: *Molecular Cloning*. 2nd edn. Cold Spring Harbor Laboratory Press, Cold Spring Harbor, NY.
64. Buechner,C.N. and Tessmer,I. (2013) DNA substrate preparation for atomic force microscopy studies of protein-DNA interactions. *J. Mol. Recognit.*, **26**, 605–617.
65. Niesen,F.H., Berglund,H. and Vedadi,M. (2007) The use of differential scanning fluorimetry to detect ligand interactions that promote protein stability. *Nat. Protoc.*, **2**, 2212–2221.
66. Ericsson,U.B., Hallberg,B.M., Detitta,G.T., Dekker,N. and Nordlund,P. (2006) Thermofluor-based high-throughput stability optimization of proteins for structural studies. *Anal. Biochem.*, **357**, 289–298.
67. Vivoli,M., Novak,H.R., Littlechild,J.A. and Harmer,N.J. (2014) Determination of protein-ligand interactions using differential scanning fluorimetry. *J. Vis. Exp.*, **91**, 51809.
68. Deppert,W. and Pates,R. (1979) Simian virus 40 specific proteins on surface of HeLa cells infected with adenovirus 2–SV40 hybrid virus Ad2+ND2. *Nature*, **277**, 322–324.
69. Deppert,W. and Pates,R. (1979) Cell surface location of simian virus 40-specific proteins on HeLa cells infected with adenovirus type 2-simian virus 40 hybrid viruses Ad2+ND1 and Ad2+ND2. *J. Virol.*, **31**, 522–536.
70. Schuck,P. (2000) Size-distribution analysis of macromolecules by sedimentation velocity ultracentrifugation and lamm equation modeling. *Biophys. J.*, **78**, 1606–1619.
71. Buechner,C.N., Heil,K., Michels,G., Carell,T., Kisker,C. and Tessmer,I. (2014) Strand-specific recognition of DNA damages by XPD provides insights into nucleotide excision repair substrate versatility. *J. Biol. Chem.*, **289**, 3613–3624.
72. Ratcliff,G.C. and Erie,D.A. (2001) A novel single-molecule study to determine protein–protein association constants. *J. Am. Chem. Soc.*, **123**, 5632–5635.
73. Roth,H.M., Romer,J., Grundler,V., Van Houten,B., Kisker,C. and Tessmer,I. (2012) XPB helicase regulates DNA incision by the Thermoplasma acidophilum endonuclease Bax1. *DNA Repair (Amst.)*, **11**, 286–293.
74. Yang,Y., Sass,L.E., Du,C., Hsieh,P. and Erie,D.A. (2005) Determination of protein-DNA binding constants and specificities from statistical analyses of single molecules: MutS-DNA interactions. *Nucleic Acids Res.*, **33**, 4322–4334.
75. Simeonov,A. (2013) Recent developments in the use of differential scanning fluorometry in protein and small molecule discovery and characterization. *Expert Opin. Drug. Discov.*, **8**, 1071–1082.
76. Hellman,L.M. and Fried,M.G. (2007) Electrophoretic mobility shift assay (EMSA) for detecting protein-nucleic acid interactions. *Nat. Protoc.*, **2**, 1849–1861.
77. Gai,D., Li,D., Finkielstein,C.V., Ott,R.D., Taneja,P., Fanning,E. and Chen,X.S. (2004) Insights into the oligomeric states, conformational changes, and helicase activities of SV40 large tumor antigen. *J. Biol. Chem.*, **279**, 38952–38959.
78. Loeber,G., Stenger,J.E., Ray,S., Parson,R.E., Anderson,M.E. and Tegtmeyer,P. (1991) The zinc finger region of simian virus 40 large T antigen is needed for hexamer assembly and origin melting. *J. Virol.*, **65**, 3167–3174.
79. Broderick,R., Rainey,M.D., Santocanale,C. and Nasheuer,H.P. (2013) Cell cycle-dependent formation of Cdc45-Claspin complexes in human cells are compromized by UV-mediated DNA damage. *FEBS J.* **280**, 4888–4902.
80. Nesper,J., Smith,R.W.P., Kautz,AR., Sock,E., Wegner,M., Grummt,F. and Nasheuer,H.P. (1997) A Cell-Free replication system for human polyomavirus JC DNA. *J. Virol.*, **71**, 7421–7428.
81. Schub,O., Rohaly,G., Smith,R.W., Schneider,A., Dehde,S., Dornreiter,I. and Nasheuer,H.P. (2001) Multiple phosphorylation sites of DNA polymerase α-primase cooperate to regulate the initiation of DNA replication in vitro. *J. Biol. Chem.*, **276**, 38076–38083.
82. Reynisdottir,I., Lorimer,H.E., Friedman,P.N., Wang,E.H. and Prives,C. (1993) Phosphorylation and active ATP hydrolysis are not required for SV40 T antigen hexamer formation. *J. Biol. Chem.*, **268**, 24647–24654.
83. Mastrangelo,I.A., Hough,P.V.C., Wilson,V.G., Waal,J.S., Hainfeld,J.F. and Tegtmeyer,P. (1985) Monomers through trimers of large tumor antigen bind in the region II of simian virus 40 origin of replication DNA as stable structures in solution. *Proc. Natl. Acad. Sci. U.S.A.*, **82**, 3626–3630.
84. Cai,L., Roginskaya,M., Qu,Y., Yang,Z., Xu,Y. and Zou,Y. (2007) Structural characterization of human RPA sequential binding to single-stranded DNA using ssDNA as a molecular ruler. *Biochemistry*, **46**, 8226–8233.
85. Kim,C., Snyder,R.O. and Wold,M.S. (1992) Binding properties of replication protein A from human and yeast cells. *Mol. Cell Biol.*, **12**, 3050–3059.
86. Kim,C., Paulus,B.F. and Wold,M.S. (1994) Interactions of human replication protein A with oligonucleotides. *Biochemistry*, **33**, 14197–14206.
87. Iftode,C., Daniely,Y. and Borowiec,J.A. (1999) Replication protein a (RPA): the eukaryotic SSB. *Critical Rev. Biochem. Mol. Biol.*, **24**, 141–180.
88. Park,C.J., Lee,J.H. and Choi,B.S. (2005) Solution structure of the DNA-binding domain of RPA from Saccharomyces cerevisiae and its interaction with single-stranded DNA and SV40 T antigen. *Nucleic Acids Res.*, **33**, 4172–4181.
89. Wang,M., Park,J.S., Ishiai,M., Hurwitz,J. and Lee,S.H. (2000) Species specificity of human RPA in simian virus 40 DNA

replication lies in T-antigen-dependent RNA primer synthesis. *Nucleic Acids Res.*, **28**, 4742–4749.
90. Weisshart,K., Taneja,P. and Fanning,E. (1998) The replication protein A binding site in simian virus 40 (SV40) T antigen and its role in the initial steps of SV40 DNA replication. *J. Virol.*, **72**, 9771–9781.
91. Huang,H., Zhao,K., Arnett,D.R. and Fanning,E. (2010) A specific docking site for DNA polymerase {alpha}-primase on the SV40 helicase is required for viral primosome activity, but helicase activity is dispensable. *J. Biol. Chem.*, **285**, 33475–33484.
92. Bochman,M.L. and Schwacha,A. (2007) Differences in the single-stranded DNA binding activities of MCM2-7 and MCM467: MCM2 and MCM5 define a slow ATP-dependent step. *J. Biol. Chem.*, **282**, 33795–33804.
93. Deb,S.P. and Tegtmeyer,P. (1987) ATP enhances the binding of simian virus 40 large T antigen to the origin of replication. *J. Virol.*, **61**, 3649–3654.
94. Eichman,B.F. and Fanning,E. (2004) The power of pumping together; deconstructing the engine of a DNA replication machine. *Cell*, **119**, 3–4.
95. Borowiec,J.A. and Hurwitz,J. (1988) Localized melting and structural changes in the SV40 origin of replication induced by T-antigen. *EMBO J.*, **7**, 3149–3158.
96. Giacherio,D. and Hager,L.P. (1979) A poly(dT)-stimulated ATPase activity associated with simian virus 40 large T antigen. *J. Biol. Chem.*, **254**, 8113–8116.
97. Pokhrel,N., Caldwell,C.C., Corless,E.I., Tillison,E.A., Tibbs,J., Jocic,N., Tabei,S.M.A., Wold,M.S., Spies,M. and Antony,E. (2019) Dynamics and selective remodeling of the DNA-binding domains of RPA. *Nature Struct Biol*, **26**, 129–136.
98. Wang,Q.M., Yang,Y.T., Wang,Y.R., Gao,B., Xi,X. and Hou,X.M. (2019) Human replication protein A induces dynamic changes in single-stranded DNA and RNA structures. *J. Biol. Chem.*, **294**, 13915–13927.
99. Deng,X., Prakash,A., Dhar,K., Baia,G.S., Kolar,C., Oakley,G.G. and Borgstahl,G.E. (2009) Human replication protein A-Rad52-single-stranded DNA complex: stoichiometry and evidence for strand transfer regulation by phosphorylation. *Biochemistry*, **48**, 6633–6643.
100. Ning,B., Feldkamp,M.D., Cortez,D., Chazin,W.J., Friedman,K.L. and Fanning,E. (2015) Simian virus Large T antigen interacts with the N-terminal domain of the 70 kD subunit of Replication Protein A in the same mode as multiple DNA damage response factors. *PLoS One*, **10**, e0116093.